AWARD NUMBER: W81XWH-16-1-0104

TITLE: The NUP98 Gene as a Potential Modifier of NF2-Associated Tumors

PRINCIPAL INVESTIGATOR: Long-Sheng Chang, Ph.D.

CONTRACTING ORGANIZATION: The Research Institute at Nationwide Children's Hospital, Columbus, Ohio 43205-2696

REPORT DATE: June 2017

TYPE OF REPORT: Annual

PREPARED FOR: U.S. Army Medical Research and Materiel Command
Fort Detrick, Maryland 21702-5012

DISTRIBUTION STATEMENT: Approved for Public Release;
Distribution Unlimited

REPORT DOCUMENTATION PAGE

Form Approved
OMB No. 0704-0188

1. REPORT DATE	2. REPORT TYPE	3. DATES COVERED
June 2017	Annual	1 Jun 2016 - 31 May 2017

4. TITLE AND SUBTITLE

The *NUP98* Gene as a Potential Modifier of NF2-Associated Tumors

5a. CONTRACT NUMBER

5b. GRANT NUMBER
W81XWH-16-1-0104

5c. PROGRAM ELEMENT NUMBER

6. AUTHOR(S)

Long-Sheng Chang, Ph.D.

E-Mail: Long-Sheng.Chang@nationwidechildrens.org

5d. PROJECT NUMBER

5e. TASK NUMBER

5f. WORK UNIT NUMBER

7. PERFORMING ORGANIZATION NAME(S) AND ADDRESS(ES)
Research Institute at Nationwide Children's Hospital
700 Children's Drive
Columbus, OH 43205-2696

8. PERFORMING ORGANIZATION REPORT NUMBER

9. SPONSORING / MONITORING AGENCY NAME(S) AND ADDRESS(ES)

U.S. Army Medical Research and Materiel Command
Fort Detrick, Maryland 21702-5012

10. SPONSOR/MONITOR'S ACRONYM(S)

11. SPONSOR/MONITOR'S REPORT NUMBER(S)

12. DISTRIBUTION / AVAILABILITY STATEMENT

Approved for Public Release; Distribution Unlimited

13. SUPPLEMENTARY NOTES

14. ABSTRACT

This exploratory hypothesis-driven award will test the hypothesis that the *NUP98* gene, which plays an important role in nucleocytoplasmic transport, gene expression, mitotic checkpoint, and pathogenesis, is frequently mutated in VS and that *NUP98* mutations are associated with disease severity. By next-generation sequencing, we previously identified missense mutations in the *NUP98* gene in VS from two NF2 patients. We now confirmed that the changes include a D1156N mutation in exon 23, a Q1142E variant also in exon 23, and a K1178R mutation in exon 24, but not in the rest of *NUP98* exons. By analyzing a total of 31 NF2-associated VS and 25 sporadic VS and by searching the COSMIC (Catalogue of Somatic Mutations in Cancer) database, we showed that NF2-associated VS have a higher incidence of harboring these mutations/variant than sporadic VS or individuals without VS. These changes are heterozygous and are present in patients' germline. Intriguingly, the amino acids affected by these *NUP98* mutations/variant are evolutionarily conserved among various species and are clustered in a coiled region of the protein. Our findings suggest that the *NUP98* exons 23 and 24 encode an important functional domain and further implicate *NUP98* as a potential genetic modifier for NF2.

15. SUBJECT TERMS
Neurofibromatosis type 2 (NF2), the *neurofibromatosis 2* (*NF2*) gene, the *nucleoporin 98* (*NUP98*) gene, vestibular schwannoma, NF2-associated, sporadic, mutation, variant, polymorphism, genetic modifier

16. SECURITY CLASSIFICATION OF:			17. LIMITATION OF ABSTRACT	18. NUMBER OF PAGES	19a. NAME OF RESPONSIBLE PERSON
a. REPORT	b. ABSTRACT	c. THIS PAGE			USAMRMC
Unclassified	Unclassified	Unclassified	Unclassified	45	19b. TELEPHONE NUMBER *(include area code)*

Table of Contents

1. Introduction

Patients with neurofibromatosis type 2 (NF2), which is characterized by a diverse array of clinical phenotypes, including bilateral vestibular schwannomas (VS) and multiple meningiomas, frequently exhibit a significant amount of phenotypic heterogeneity. These patients often show differences in clinical presentation and tumor number as well as unpredicted tumor growth rates. Presently, the causes of this clinical variability are not understood. While loss of the *neurofibromatosis type 2* (*NF2*) tumor suppressor gene plays an important role in tumor development, it is likely that additional genes may contribute to NF2 pathogenesis and/or clinical heterogeneity. To identify if any other genes that are frequently mutated in NF2-associated tumors, we previously analyzed 405 cancer-related genes in VS from two NF2 patients with large, fast-growing tumors by next-generation sequencing using the FoundationOne Heme test. In addition to alterations in the *NF2* gene, mutations were also found in the *nucleoporin 98* (*NUP98*) gene in both patients' VS. As a component of the nuclear pore complex, the NUP98 protein participates in nucleocytoplasmic transport. In addition, NUP98 has been shown to play important roles in gene expression, mitotic checkpoint, and pathogenesis. Furthermore, alterations in the *NUP98* gene have been found in several types of human cancer. By analyzing blood samples from these NF2 patients, we have confirmed the presence of *NUP98* mutations in these patients' germline. Intriguingly, the amino acid residues affected by the *NUP98* mutations that we identified are evolutionarily conserved among various species, implying that these residues may be important for protein function. The objective of this Exploratory Hypothesis-Driven Award is to further examine whether the *NUP98* gene is frequently mutated in NF2 patients and whether *NUP98* mutations are associated with disease severity.

2. Keywords

Neurofibromatosis type 2 (NF2), *neurofibromatosis 2* (*NF2*) gene, *NUP98* gene, vestibular schwannoma, NF2-associated, sporadic, mutation, variant, polymorphism, genetic modifier.

3. Accomplishments

(I) The major goals of this project are to (1) determine the frequency of *NUP98* mutations in a large cohort of patients with NF2-associated and sporadic VS and in individuals without a history of VS and (2) correlate the presence of *NUP98* mutation with clinical parameters, such as tumor size, growth rate, and tumor recurrence.

(II) Accomplishment under these goals:

(1) By next-generation sequencing of VS from two NF2 patients using the FoundationOne Heme test, we previously identified *NUP98* mutations in both patients' tumors. The first patient's VS carried a K1178R mutation in exon 24 of the *NUP98* gene and the second patient's VS had a D1156N mutation in exon 23. To confirm these data, we analyzed blood and tumor DNA samples from these two patients by polymerase chain reaction (PCR) and DNA sequencing. We confirmed that both the blood and tumor from patient #1 had a heterozygous K1178R mutation in exon 24 but did not have the D1156N mutation in exon 23. However, we did detect another nucleotide change in exon 23, resulting in an amino acid change on Q1142E in this patient #1's blood and tumor DNA. Also, we confirmed that both the blood and tumor DNA from patient's #2 harbored a heterozygous D1156N mutation in exon 23 but did not have any changes for Q1142E in exon 23 or K1178R in exon 24. These results indicate that the K1178R and D1156N mutations were present in the germline of these two NF2 patients. Further analysis of blood samples from the parents of these NF2 patients revealed that the K1178R mutation found in patient #1 and the D1156N mutation found in patient #2 were inherited from one of their parents.

(2) To verify whether the K1178R and D1156N changes are true mutations, we first

searched the COSMIC (Catalogue of Somatic Mutations in Cancer) database. We found that mutations in the *NUP98* gene was detected in approximately 0.5~1% of human cancers and that the most common types of changes (~80%) were missense mutations (http://cancer.sanger.ac.uk/cosmic/gene/analysis?ln=NUP98). Note that the *NUP98* mutations we identified in these NF2-associated VS were missense mutations. From searching the SNP database in NCBI, we found that the D1156N C→T change in exon 23 (http://www.ncbi.nlm.nih.gov/projects/SNP/snp_ref.cgi?rs=149421589) and the K1178R A→G change in exon 24 (http://www.ncbi.nlm.nih.gov/projects/SNP/snp_ref.cgi?rs=779147191) have never been observed among more than 120,000 individuals analyzed, while the Q1142E G→C change (http://www.ncbi.nlm.nih.gov/projects/SNP/snp_ref.cgi?rs=35404087) were found in ~8% of population. These results suggest that the D1156N and K1178R changes likely represent true mutations, while the Q1142E change may be considered as a genetic variant. Nonetheless, the significance for these *NUP98* mutations or variant in NUP98 biology or in NF2 pathogenesis has not been studied.

(3) To examine whether there are any mutations in exons other than exons 23 and 24 of the *NUP98* gene, we performed PCR analysis on all 33 *NUP98* exons using genomic DNA isolated from NF2-associated VS. Sequencing analysis of PCR products revealed that mutations were not identified in the remaining 31 exons in the tumors (Figure 1). Using I-TASSER (Iterative Threading ASSEmbly Refinement) for protein structure and function prediction (http://zhanglab.ccmb.med.umich.edu/I-TASSER/), it predicts that the *NUP98* gene product to be an α-helical solenoid and that the D1156N and K1178R mutations as well as Q1142E variant are clustered in a coiled region of the protein (data not shown). Together with the evolutionary conservation of these three amino acid residues among various species, these results suggest that the *NUP98* exons 23 and 24, which encode these amino acid residues, may harbor an important functional domain and support the notion that *NUP98* may be a genetic modifier for NF2.

Figure 1. Mutations were not found in exons other than exons 23 and 24 of the *NUP98* gene in NF2-associated VS. Alignment of the sequences of exons 21, 22, 25, 28, 30, and 31 of the *NUP98* gene detected in the VS from NF2 patient #1 with the corresponding exon sequences of the wild-type *NUP98* gene was performed, and identical sequences were found in all these exons.

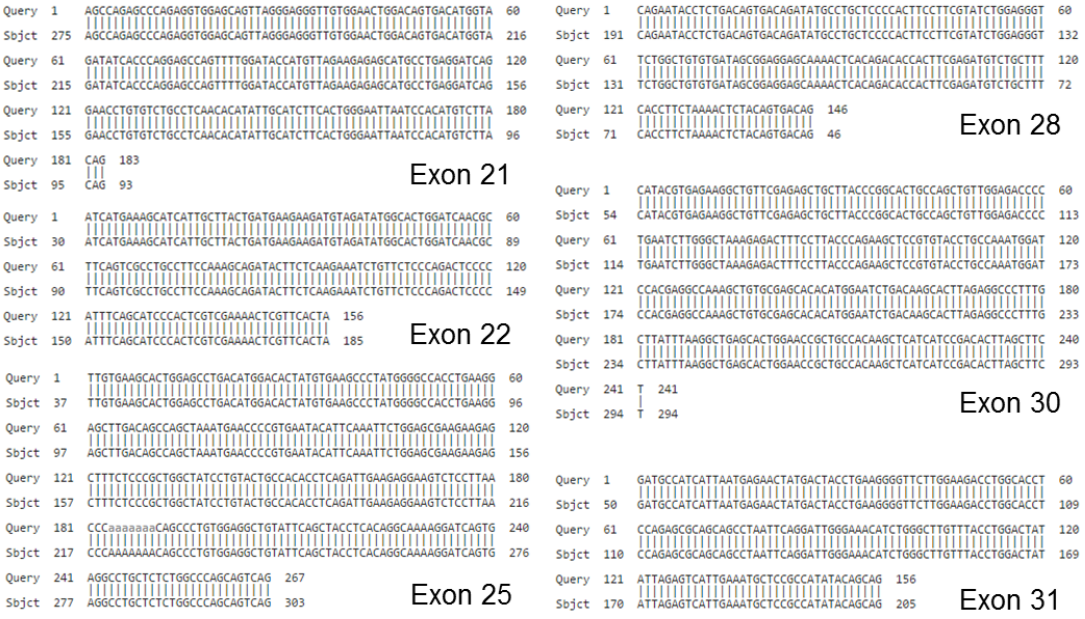

(4) We have analyzed additional 12 NF2-associated and 11 sporadic VS and 10 blood samples from individuals without VS for *NUP98* mutations. We found that including the first two NF2 patients described above, 8/14 (57%) NF2 patients carried one or two of the three changes identified in *NUP98* (Q1142E, D1156N, and K1178R). Even if we only consider the D1156N and K1178R mutations, 3/14 (21%) NF2 patients carried these changes (Table 1). On the contrary, we found only 1/11 (9%) patients with sporadic VS harbored the Q1142E change and none of the 10 individual without VS had any of the three changes identified. As in the first two NF2 patients, all of these three changes detected were heterozygous.

Table 1. Frequency of *NUP98* mutations in NF2 patients, sporadic VS patients, and individuals without VS identified at The Ohio State University.

Mutation	Amino acid change	Frequency		
		NF2 patients*	Sporadic VS*	Non-VS
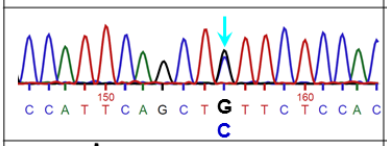	Q1142E (G→C change in exon 23)	6/14 (43%)	1/11 (9%)	0/10 (0%)
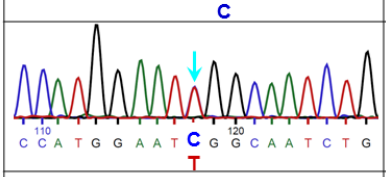	D1156N (C→T change in exon 23)	1/14 (7%)	0/11 (0%)	0/10 (0%)
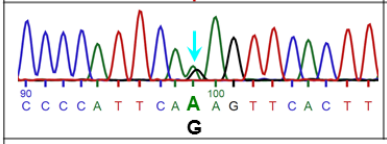	K1178R (A→G change in exon 24)	2/14 (14%)	0/11 (0%)	0/10 (0%)
Total number of patients with any of the three changes Total number of patients with D1156N or K1178R changes		8/14† (57%) 3/14 (21%)‡	1/11 (9%) 0/11 (0%)‡	0/10 (0%) 0/10 (0%)‡

*Analysis was performed on VS and/or blood DNA; †One patient exhibited two changes (K1178R and Q1142E); ‡the frequency shown if only considering D1156N and K1178R mutations.

Figure 2. Detection of a polymorphism/silent change in exon 23 of the *NUP98* gene in NF2 patients, sporadic VS patients, and individuals without VS.

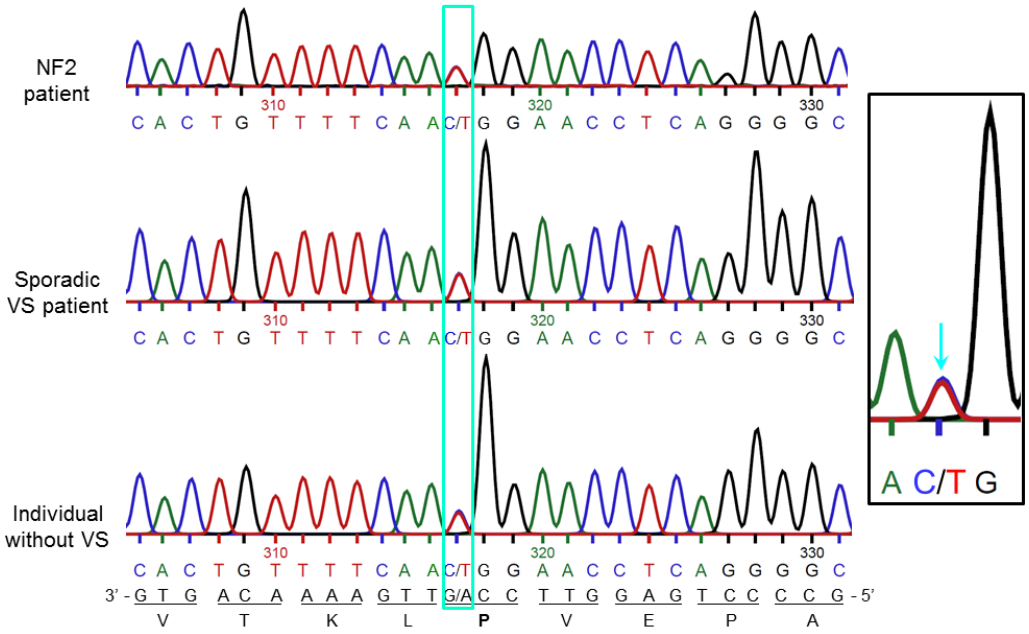

Furthermore, unlike the Q1142E, D1156N, and K1178R changes, we detected a

nucleotide polymorphism in the *NUP98* exon 23, which does not change the encoded amino acid (a silent change), in NF2 patients, sporadic VS patients, and individuals without NF2 at a similar frequency (Figure 2) This is in contrast to the higher frequencies of the Q1142E, D1156N, and K1178R changes detected in NF2 patients (Table1).

In addition, we have established a collaboration with Dr. Miriam Smith at the University of Manchester to investigate the NF2-associated and sporadic VS procured in the UK NF2 Registry. She has examined 17 blood-tumor pairs from NF2 patients and 14 blood-tumor pairs from sporadic VS patients and found that 4/17 (24%) NF2 patients each carried the Q1142E and D1156N changes in exon 23, while only 1/14 (7%) sporadic VS harbored the Q1142E change. Similar to those detected by us, both the Q1142E and D1156N changes detected by the UK group were heterozygous.

Taken together, we conclude that NF2 patients are more frequently to carry the Q1142E variant and/or the D1156N and K1178R mutations.

(5) To achieve a significant statistical comparison on the prevalence of *NUP98* mutations in NF2-associated and sporadic VS and in individuals without VS, we have continued to procure VS specimens. Over the past year, we obtained three additional NF2-associated and more than 20 sporadic VS. Also, we collected blood samples from some of these patients. We have prepared DNA from these tumors and are in the process of analyzing these samples for *NUP98* mutations.

(6) As we have been routinely procuring fresh VS tumors, we have also used them to prepared primary VS cultures for therapeutic evaluation. We have published a methodology paper describing the use of schwannoma and meningioma cells to establish noninvasive, quantifiable, orthotopic animal models (Burns and Chang, 2016; see Appendices). In addition, we have collaborated with Dr. Cristina Fernandez-Valle at the University of Central Florida to study the effect of ponatinib, an FDA-approved ABL/SRC inhibitor, on proliferation and survival of merlin-deficient human Schwann and schwannoma cells. The study shows that ponatinib effectively inhibits the growth of merlin-deficient cells and suggest that it should be further evaluated as a potential therapeutic agent for NF2-associated schwannomas (Petrilli et al., 2017; see Appendices).

(III) Opportunities for training and professional development:

This project was not intended to provide training and professional development opportunities; therefore, we have "Nothing to Report."

(IV) How were the results disseminated to communities of interest?

Nothing to report.

(IV) Plan to do during the next reporting period to accomplish the goals:

We will continue to procure more VS specimens and use them for *NUP98* mutational analysis in the second year. In addition, we will begin to collect clinical information regarding tumor size, growth rate, age of diagnosis, and onset of symptoms for correlation analysis to determine whether *NUP98* mutations contribute to the severity of NF2-associated VS.

4. Impact

(I) Impact on the development of the principal discipline(s) of the project:

We have confirmed the presence of *NUP98* mutations in NF2-associated VS and a higher prevalence of *NUP98* mutations in NF2 patients compared to sporadic VS patients or

individuals without VS. Further analysis of the potential clinical implications of *NUP98* mutations may allow us to better understand the phenotypic heterogeneity among NF2 patients. Identification of *NUP98* as a genetic modifier for NF2 will substantially enhance our understanding of the disease characteristics and pathobiology as well as future drug discovery.

(II) Impact on other disciplines:
Nothing to report.

(III) Impact on technology transfer:
Nothing to report.

(IV) Impact on society beyond science and technology:
Nothing to report.

5. Changes/Problems
Nothing to report.

6. Products

(I) Publications, conference papers, and presentations

(1) Journal publications

The works described in the following two papers published during the past year were supported, in part, by this grant. We have acknowledged this grant support in these publications (please see Appendices)

(i) Burns SS, Chang L-S. 2016. Generation of noninvasive, quantifiable, orthotopic animal models for NF2-associated schwannoma and meningioma. Methods Mol Biol. 1427:59-72. PMID: 27259921

The development of preclinical animal models that accurately capture the clinical characteristics of NF2-associated schwannomas and meningiomas will facilitate the evaluation of novel therapeutic agents for the treatment of these tumors, ultimately leading to more productive clinical trials. In this methodology paper, we describe the generation of luciferase-expressing *NF2*-deficient schwannoma and meningioma cells and the use of these cells to establish orthotopic, quantifiable tumor models in immunodeficient mice. The growth of these tumors and their response to treatment can be measured effectively by bioluminescence imaging (BLI) and confirmed by small-animal magnetic resonance imaging (MRI). These and other animal models, such as genetically-engineered models, should substantially advance the investigation of promising therapies for schwannomas and meningiomas.

(ii) Petrilli AM, Garcia J, Bott M, Klingeman Plati S, Dinh CT, Bracho OP, Yan D, Zou B, Mittal R, Telischi FF, Liu X-Z, Chang L-S, Welling DB, Copik AJ, Fernández-Valle C. 2017. Ponatinib Promotes a G1 Cell Cycle Arrest of Merlin/NF2-Deficient Human Schwann Cells. Oncotarget 8:31666-31681. PMID: 28427224. PMCID: PMC5458238

This collaborative publication reported the effect of ponatinib, an FDA-approved ABL/SRC inhibitor, on proliferation and survival of merlin-deficient human Schwann and schwannoma cells. We have established a collaboration with Dr. Cristina Fernandez-Valle at the University of Central Florida to use paired human vestibular schwannoma and normal vestibular nerve specimens that we procured to confirm elevated levels of phosphorylated PDGFRα/β, and SRC in merlin-deficient tumor

cells. Dr. Fernandez-Valle's group further showed that ponatinib reduced the viability of merlin-deficient Schwann cells by decreasing phospho-PDGFRα/β and ERK1/2 and their downstream signals. These changes were associated with decreased cyclin D1 and increased $p27^{KIP1}$ levels, leading to a G_1 cell-cycle arrest. These results suggest that ponatinib is a potential therapeutic agent for NF2-associated schwannomas.

(2) Abstracts presented at national/international conferences

The following five abstracts were presented at the annual Neurofibromatosis (NF) Conferences last year and this year. We have acknowledged this grant support in these abstracts (please see Appendices).

(i) Burns, S.S., E.M. Akhmametyeva, J. Blakeley, D.B. Welling, L.-S. Chang. 2016. Similarities and Differences in Tumor Characteristics and Treatment Response in NF2-Associated Vestibular Schwannomas and Meningiomas. The 2016 NF Conference, Austin, TX.

(ii) Oblinger, J., S. Burns, M. Curley, L.-S. Chang. 2016. ErbB3 and IGF-1R blockade as a potential treatment for vestibular schwannomas and meningiomas. The 2016 NF Conference, Austin, TX.

(iii) Oblinger, J., Burns, S., Kinghorn, A.D. , Chang, L.-S. 2017. Natural Silvestrol-Related Rocaglates as Potential Treatments for Vestibular Schwannomas and Meningiomas. The 2017 NF Conference, Washington, DC.

(iv) Burns, S., Oblinger, J., Akhmametyeva, E., Welling, D.B., Chang, L.-S. 2017. A strategy to identify an effective therapy for NF2-associated vestibular schwannomas. The 2017 NF Conference, Washington, DC.

(v) Chang, L.-S., Huang, J., Akhmametyeva E., Burns, S. 2017. Merlin plays an important role in centrosome disjunction. The 2017 NF Conference, Washington, DC.

7. Participants & Other Collaborating Organizations

(i) Individuals who have worked on the project

Long-Sheng Chang, Principal Investigator – No change
Sarah Burns, Research Assistant – No change

(ii) Has there been a change in the active other support of the PD/PI(s) or senior/key personnel since the last reporting period?

Nothing to report.

(iii) What other organizations were involved as partners

Collaborator: Dr. Miriam J. Smith, Ph.D., Lecturer in Cancer Genomics, Centre for Genomic Medicine, Institute of Human Development, University of Manchester
5th Floor, St Mary's Hospital, Oxford Road, Manchester M13 9WL, UK

To ensure that a sufficient number of VS specimens are analyzed, we have established a collaboration with Dr. Miriam Smith at The University of Manchester where the UK NF2 registry is based. As mentioned above, their preliminary study also identified *NUP98* mutations/variant in VS, particularly those associated with NF2.

8. Special Reporting Requirement
Not applicable.

9. Appendices (see attached)
Two peer-reviewed publications

(1) Burns SS, Chang L-S. 2016. Generation of noninvasive, quantifiable, orthotopic animal models for NF2-associated schwannoma and meningioma. Methods Mol Biol. 1427:59-72. PMID: 27259921

(2) Petrilli AM, Garcia J, Bott M, Klingeman Plati S, Dinh CT, Bracho OP, Yan D, Zou B, Mittal R, Telischi FF, Liu X-Z, Chang L-S, Welling DB, Copik AJ, Fernández-Valle C. 2017. Ponatinib Promotes a G1 Cell Cycle Arrest of Merlin/NF2-Deficient Human Schwann Cells. Oncotarget 8:31666-31681. PMID: 28427224. PMCID: PMC5458238

Five abstracts presented at national conferences

(i) Burns, S.S., E.M. Akhmametyeva, J. Blakeley, D.B. Welling, L.-S. Chang. 2016. Similarities and Differences in Tumor Characteristics and Treatment Response in NF2-Associated Vestibular Schwannomas and Meningiomas. The 2016 NF Conference, Austin, TX.

(ii) Oblinger, J., S. Burns, M. Curley, L.-S. Chang. 2016. ErbB3 and IGF-1R blockade as a potential treatment for vestibular schwannomas and meningiomas. The 2016 NF Conference, Austin, TX.

(iii) Oblinger, J., Burns, S., Kinghorn, A.D. , Chang, L.-S. 2017. Natural Silvestrol-Related Rocaglates as Potential Treatments for Vestibular Schwannomas and Meningiomas. The 2017 NF Conference, Washington, DC.

(iv) Burns, S., Oblinger, J., Akhmametyeva, E., Welling, D.B., Chang, L.-S. 2017. A strategy to identify an effective therapy for NF2-associated vestibular schwannomas. The 2017 NF Conference, Washington, DC.

(v) Chang, L.-S., Huang, J., Akhmametyeva E., Burns, S. 2017. Merlin plays an important role in centrosome disjunction. The 2017 NF Conference, Washington, DC

Chapter 4

Generation of Noninvasive, Quantifiable, Orthotopic Animal Models for NF2-Associated Schwannoma and Meningioma

Sarah S. Burns and Long-Sheng Chang

Abstract

Schwannomas and meningiomas are nervous system tumors that can occur sporadically or in patients with neurofibromatosis type 2 (NF2). Mutations of the *Neurofibromatosis 2* (*NF2*) gene are frequently observed in these tumors. Schwannomas and meningiomas cause significant morbidities, and an FDA-approved medical therapy is currently not available. The development of preclinical animal models that accurately capture the clinical characteristics of these tumors will facilitate the evaluation of novel therapeutic agents for the treatment of these tumors, ultimately leading to more productive clinical trials. Here, we describe the generation of luciferase-expressing *NF2*-deficient schwannoma and meningioma cells and the use of these cells to establish orthotopic tumor models in immunodeficient mice. The growth of these tumors and their response to treatment can be measured effectively by bioluminescence imaging (BLI) and confirmed by small-animal magnetic resonance imaging (MRI). These and other animal models, such as genetically-engineered models, should substantially advance the investigation of promising therapies for schwannomas and meningiomas.

Key words Vestibular schwannoma, Meningioma, Neurofibromatosis type 2 (NF2), *Neurofibromatosis 2* (*NF2*) gene, Xenograft, Allograft, Severe combined immunodeficiency (SCID) mice, Intranerve, Stereotactic, Bioluminescence imaging (BLI), Magnetic resonance imaging (MRI)

1 Introduction

Vestibular schwannomas (VS) are tumors originating from Schwann cells covering the vestibular branch of the 8th cranial nerve. These tumors are often slow-growing and can occur sporadically or in association with neurofibromatosis type II (NF2; OMIM #101000), a highly penetrant, autosomal-dominant genetic disorder [1]. Nearly all NF2 patients develop bilateral VS, and up to 60 % of these patients develop meningiomas. Other disease features include ependymomas, spinal schwannomas, astrocytomas, and presenile lens opacities. Patients with VS usually present with tinnitus, hearing loss, and imbalance. These tumors can lead to deafness, facial nerve paralysis, brainstem compression, hydrocephalus, and death, if left untreated.

Bernd Sokolowski (ed.), *Auditory and Vestibular Research: Methods and Protocols*, Methods in Molecular Biology, vol. 1427,
DOI 10.1007/978-1-4939-3615-1_4,

Meningiomas are derived from cells of the meninges lining the brain. About 80 % of meningiomas are benign (WHO grade I), whereas the remaining are atypical (grade II) and anaplastic (grade III) [2]. These tumors cause significant morbidity, including cranial nerve palsy, seizures, and brainstem compression, which may lead to paralysis, aspiration pneumonia, and death. Approximately 20 % of benign meningiomas recur over ten years, while grade II and grade III tumors possess greater rates of recurrence. Meningiomas in NF2 patients are associated with disease severity and increased risk of mortality [3, 4].

Currently, an FDA (U.S. Food and Drug Administration)-approved drug is not available for the treatment of VS and meningiomas. Treatment options for these tumors are presently limited to observation, surgical removal, and stereotactic radiation [1]. However, surgery may not be possible if the tumor is inaccessible or when there are too many tumors. Radiation treatment may cause malignant transformation and/or growth acceleration of benign tumor cells. In addition, preservation of hearing and balance along with the facial nerve and lower cranial nerves for swallowing and airway protection are often not achieved with current methods. Together, these factors underscore the importance of developing effective medical therapies that stop tumor growth.

Evaluation of potential novel therapeutic agents requires animal models that accurately reflect disease characteristics. Most, if not all, of NF2-associated VS and the more common sporadic unilateral schwannomas harbor mutations in the *Neurofibromatosis 2* (*NF2*) tumor suppressor gene [5, 6]. Additionally, *NF2* mutations are found in most NF2-associated meningiomas and about 50–60 % of sporadic meningiomas [4, 7, 8]. To address the tumor suppressor role of merlin, mice that lack *Nf2* function in Schwann or meningeal cells have been generated and develop schwannomas and meningiomas, respectively [9–11]. These genetically engineered mouse (GEM) models have been used in therapeutic evaluation; however, tumor latency, penetrance, and detection in these GEM models are important considerations. Also, xenograft models in severe combined immunodeficiency (SCID) mice implanted with VS specimens have been established, but the tumors do not exhibit consistent growth [12, 13]. Thus, additional models that closely mimic the clinical presentation of *NF2*-deficient benign schwannomas and meningiomas and that facilitate efficient quantitation of tumor growth will further enhance therapeutic testing.

Accurate measurement of tumor size and longitudinal monitoring of tumor growth are critical in evaluating drug responses. Magnetic resonance imaging (MRI) has been the gold standard for evaluating NF2-associated tumors in situ [14]. Likewise, small-animal MRI has been used to noninvasively monitor tumor growth in mouse models. To facilitate longitudinal monitoring of

drug response, bioluminescence imaging (BLI) has significantly advanced the ability to quantitate tumor growth in animal models and is particularly valuable for intracranial tumors whose growth cannot be monitored externally [15]. Here, we describe the use of luciferase-expressing schwannoma and meningioma cells to generate orthotopic animal models. Tumor growth in these models can be quantified over time by BLI and confirmed by MRI.

2 Materials

2.1 Cell Culture

1. Dulbecco's modified Eagle (DME) and DME/F-12 (v/v) media (Life Technologies, Grand Island, NY) are supplemented with 10 % fetal bovine serum (FBS).
2. 100× Penicillin/Streptomycin stock solution: Mix 5000 units/ml penicillin G sodium and 5000 μg/ml streptomycin sulfate in 0.85 % saline (*see* **Note 1**).
3. Phosphate-buffered saline (PBS) without Ca^{2+}/Mg^{2+}: 137 mM NaCl, 2.7 mM KCl, 10 mM Na_2HPO_4, and 1.8 mM KH_2PO_4, pH 7.4.
4. Tris-buffered saline (TBS): 50 mM Tris–HCl, pH 7.4 and 150 mM NaCl.
5. Trypsin solution: 0.25 % trypsin-0.53 mM EDTA in Hanks' Balanced Salt Solution (HBSS).
6. Reconstitute recombinant human neuregulin-β1/heregulin-β1 epidermal growth factor domain (rhuHRG-β1) in PBS, aliquot in small volumes, and store at −80 °C.
7. Forskolin stock solution: Prepare 5 mM forskolin in dimethyl sulfoxide (DMSO), sterilize using a 0.2-μm filter, aliquot, and store at −20 °C. HRG-β1 and forskolin are freshly added to culture medium (*see* Subheading 3.1, **step 1**).
8. 100× Poly-L-lysine or Poly-D-lysine (molecular weight 75–150 kDa) stock solution: Prepare 5 mg/ml in TBS and store at 4 °C.
9. 250× Laminin stock: Purchased as 1 mg/ml solution from, e.g., Sigma and stored at −80 °C.
10. *Nf2*^{P0} (*P0Cre;Nf2*$^{flox/flox}$) schwannoma cells.
11. *Nf2*^{P0} schwannoma cell culture medium: DME/F-12 medium supplemented with 10 % FBS, 10 ng/ml HRG-β1, and 2 μM forskolin.
12. *NF2*-deficient benign human meningioma cell line Ben-Men-1.
13. Ben-Men-1 culture medium: Supplement DME medium with 10 % FBS.

2.2 Lentiviral Transduction and Isolation of Luciferase-Expressing Clones

1. Lenti-CMV-Luc lentiviruses containing a cytomegalovirus (CMV) promoter-driven luciferase-expression unit and a puromycin-resistance gene (Qiagen, Germantown, MD).
2. 10,000× Polybrene (hexadimethrine bromide; Sigma-Aldrich) solution: Prepare polybrene by dissolving 80 mg in 1 ml of H_2O, sterilize by filtration, and store at 4 °C (*see* **Note 5**).
3. Puromycin dihydrochloride stock solution: Prepare a 5 mg/ml solution in DME medium, sterilize by filtration, aliquot, and store at −20 °C (*see* Subheading 3.2, **step 5**).
4. Cloning cylinders (Bellco Glass, Vineland, NJ) are used to isolate individual puromycin-resistant colonies.
5. The Protein Assay Dye Reagent Concentrate (Bio-Rad, Hercules, CA) is diluted five-fold prior to protein concentration measurements (*see* Subheading 3.2, **step 7**).
6. The Luciferase Reporter Assay System (Promega, Madison, WI) is used according to the manufacturer's instruction.
7. A SpectraMax microplate reader (Molecular Devices, Sunnyvale, CA) is used to detect luciferase activity in cultured cells (*see* Subheading 3.2, **step 8**).

2.3 Mice and Tumor Cell Injection

1. SCID C.B17 mice are purchased from a certified vendor, such as The Jackson Laboratory, Charles River Laboratories, and Taconic Biosciences (*see* Subheadings 3.3 and 3.4, **step 3**).
2. PROTEXIS sterile powder-free surgical gloves, Curity™ gauze sponges, Webcol™ alcohol prep, and Duo-Swab® Povidone-Iodine Cleansing Scrub and Prep Swabsticks.
3. Isoflurane (Forane) and an Inhalation Anesthesia System and Vapor Guard activated charcoal adsorption filters (VET Equip® Instrument, Livermore, CA).
4. Fine surgical instruments, including iris scissors, forceps, scalpels, blades, and a high-speed micro drill with carbon steel burrs (0.5 mm diameter) (Fine Science Tools, Foster City, CA).
5. A Mini ARCO hair clipper (Wahl Clipper Corp, Sterling, IL).
6. A model 940 small-animal stereotaxic instrument with a BENCHMark™ 3-axes digital counter display (Leica Biosystems, Inc., Buffalo Grove, IL) equipped with an inhalation anesthesia system (VET Equip® Instrument) and a KDS310 Nano single syringe infusion/withdraw pump (KD Scientific, Holliston, MA).
7. Hamilton Neuros™ 10 μl syringes with removable 33-gauge or 26-gauge needles are used for intranerve or intracranial injection, respectively.
8. An OPMI Pro Magis surgical microscope (Carl Zeiss Microscopy, LLC, Thornwood, NY).

9. Vetbond™ tissue adhesive (3M, St. Paul, MN).
10. Small-animal thermo-controlled recovery pads, to enhance post-surgical recovery.

2.4 Bioluminescence Imaging

1. D-luciferin potassium stock: D-luciferin potassium salt (Gold Biotechnology, St. Louis, MO) is dissolved as a 15 mg/ml stock in PBS. The stock solution should be sterilized by filtration. Alternatively, a ready-to-inject solution of D-luciferin (Xenolight RediJect; Perkin Elmer, Waltham, MA) is also available (*see* Subheading 3.5, **step 1**).
2. Insulin syringes with 28-gauge needles are used for luciferin injection into mice.
3. An IVIS Spectrum Preclinical In Vivo Imaging System and Living Image® software (Perkin Elmer) (*see* Subheading 3.5, **step 4**).
4. Isoflurane (Forane) is used to anesthetize mice throughout the imaging process.

3 Methods

Orthotopic animal models of tumors are essential tools in evaluating the safety and efficacy of potential therapeutics. These models can complement cell culture models by providing the native environment for tumor growth on the organismal level. In addition, they facilitate assessment of drug distribution and the ability of a drug to reach the tumor tissue and to inhibit target molecules. Effective animal models accurately recapitulate the specific features of the human tumors. As benign schwannomas and meningiomas tend to be slow-growing, an ideal animal model for these tumors would incorporate this growth characteristic. We discuss approaches for generating orthotopic, quantifiable schwannoma allograft and meningioma xenograft models, which can be used to evaluate potential therapeutic agents.

3.1 Schwannoma and Meningioma Cell Cultures

1. Dissect and use schwannomas developed in *P0Cre;Nf2$^{flox/flox}$* (*Nf2^{P0}*) mice with conditional *Nf2* inactivation in Schwann cells [9] to prepare schwannoma cell cultures as described previously [16].
2. Grow *Nf2^{P0}* schwannoma cells in DME/F-12 (*see* Subheading 2.1, **step 5**) and plate on dishes coated with polylysine and laminin.
3. Confirm *Nf2*/Merlin status of these schwannomas by PCR genotyping and Western blotting [16, 17] (*see* **Note 2**).
4. Grow *NF2*-deficient benign human meningioma cell line Ben-Men-1 in DME medium supplemented with 10 % FBS on non-coated dishes [18, 19] (*see* **Note 3**).

3.2 Generation of Luciferase-Expressing Sch10545-Luc Schwannoma and Ben-Men-1-LucB Meningioma Cells

1. Trypsinize and plate Sch10545 schwannoma (derived from an *Nf2*^{p0} mouse) and Ben-Men-1 meningioma cells in fresh growth medium so that they will be about 25–50 % confluent by the next day. An extra dish of cells is plated at the same dilution to determine the number of cells in the dish.
2. The next day, trypsinize and count cells in the extra dish to determine the amount of lentivirus needed for infection (*see* **Note 4**). We usually infect Sch10545 or Ben-Men-1 cells with Lenti-CMV-Luc lentiviruses at a multiplicity of infection (MOI) of 1 to 10 (*see* **Note 5**). The MOI is defined as the number of infectious viral particles per cell (*see* **Note 6**).
3. For lentiviral transduction, remove medium from the dish. Based on the number of cells determined, mix an appropriate amount of lentiviruses with growth media supplemented with 8 μg/ml of polybrene and add to the cells. Incubate dish at 37 °C from 4 h to overnight (*see* **Note 7**).
4. Change media the next day following transduction and incubate the transduced dish at 37 °C for another day.
5. Two days after transduction, add puromycin to the cells to a final concentration of 2 μg/ml and replenish the growth medium containing puromycin every 3 days until puromycin-resistant colonies are visible (*see* **Note 8**)
6. Isolate individual puromycin-resistant colonies using cloning cylinders and expand in separate dishes containing growth medium and puromycin (*see* **Note 9**).
7. Trypsinize cells when dishes containing individual puromycin-resistant clones approach confluence. Expand half of the cells from each clone into a new dish to continue propagating as a stock. Wash the other half of the cells with PBS 2× and lyse in the Luciferase Reporter Lysis Buffer (Subheading 2.2, **step 6**). To determine the protein concentration, mix 2 μl of each clear lysate with 1 ml of diluted Bio-Rad Protein Assay Dye Reagent (*see* Subheading 2.2, **step 5**) and measure the absorbance at a wavelength of 595 nm. Generate a standard curve for protein concentration by measuring the absorbance of a series of standards with known amounts of protein at 595 nm and use these data to extrapolate each sample's protein concentration.
8. Measure luciferase activity by using equal amounts of proteins from each lysate (10 μg) using a Promega Luciferase Assay Kit and a microplate reader, according to the manufacturer's instructions. Inject clones expressing robust luciferase activity (e.g., Sch10545-Luc and Ben-Men-1-LucB) into mice to generate luciferase-expressing schwannoma allograft and meningioma xenograft tumors as described in the following sections.

3.3 Intranerve Injection of Luciferase-Expressing Mouse *Nf2*$^{-/-}$ Schwannoma Cells into the Nerves of SCID Mice

1. Acquire approval from the institutional animal care and use committee (IACUC) prior to initiating any studies involving animals.
2. Trypsinize and count actively-growing, luciferase-expressing Sch10545-Luc schwannoma cells. Wash in PBS 2× and spin down at 2000 × *g* for 30 s in an Eppendorf microfuge. Resuspend cell pellet in an appropriate volume of PBS and place on ice until injection. To establish schwannoma allografts, inject ~10^5 Sch10545-Luc cells in 3 μl of PBS per mouse.
3. To perform intranerve injections, anesthetize an 8-to-10-month-old SCID mouse (*see* **Note 10**) using 5 % isoflurane in oxygen in an induction chamber until it is under deep anesthesia and does not respond to toe pinches. The induction chamber is connected to an Inhalation Anesthesia System to regulate isoflurane flow rate and to a Vapor Guard activated charcoal adsorption filter to capture the waste gas.
4. Once anesthetized, place the mouse on its stomach with its hind legs outstretched on a clean surgical platform. To maintain anesthesia during surgery, place a nose cone connected to an Inhalation Anesthesia System on the nose to continue administering isoflurane gas. Use a mini-hair clipper to remove hair from the right (or left) thigh and hind leg area, since only one sciatic nerve is injected with cells (*see* **Note 11**).
5. Disinfect the surgical site with a Povidone-Iodine Cleansing Scrub Swabstick and then with a Povidone-Iodine Antiseptic Prep Swabstick. Make a small incision (~1 cm) in the skin of the flank just below and parallel to the femur. Use scissors to separate the skin from the muscle of the leg. To expose the sciatic nerve, blunt dissect through the biceps femoris muscle using a pair of sharp scissors. The sciatic nerve should appear as a white fascicle of nerve fibers extending parallel to the femur.
6. To access the sciatic nerve for intranerve injection, insert a pair of fine forceps underneath the nerve to gently elevate and stabilize the nerve above the muscle. Load 3 μl of the Sch10545-Luc cell suspension in a Hamilton Neuros™ 10 μl syringe with a 33-gauge needle. To inject the cells, the needle of the Neuros™ syringe should be carefully inserted into the nerve by positioning the needle along the nerve. Gradually inject the contents of the syringe into the nerve, while holding the needle steady.
7. Once the syringe is empty, remove the needle slowly and place the nerve back into its original position beneath the muscle. Close and seal the incision using Vetbond™ tissue adhesive. Give the mouse a dose of buprenorphine (0.05 mg/kg) subcutaneously as an analgesic, remove the isoflurane nose cone, and place the animal on a thermo-controlled recovery pad until fully recovered and ambulatory.

3.4 Stereotactic Injection of Luciferase-Expressing NF2-Deficient Benign Meningioma Cells to the Skull Base of SCID Mice

1. As in Subheading 3.3, all animal experiments should be approved by the IACUC before initiating any studies.
2. Harvest actively-growing, luciferase-expressing Ben-Men-1-LucB for injection as described in Subheading 3.3, **step 2**. We find that injection of approximately 10^6 cells suspended in 5 μl of PBS per mouse results in reproducible establishment of intracranial tumors.
3. As in Subheading 3.3, **step 3**, anesthetize 8–12-month-old SCID mice using 5 % isoflurane in oxygen until they are under deep anesthesia and do not respond to toe pinches.
4. Stabilize the anesthetized mouse on a secure platform and position in a small-animal stereotaxic device using a nose cone connected to an Inhalation Anesthesia System. Insert the ear pins carefully into the ear canals. When positioned properly, the head of the mouse is immobilized to minimize movement of the head during stereotactic injection.
5. Remove the hair on the top of the head using a pair of iris scissors and cleanse the surface area of the head from the nose to the back of the skull with Duo-Swab® Povidone-Iodine Cleansing Scrub and Antiseptic Prep Swabsticks. Using a scapel with a No. 10 surgical blade, make a longitudinal midline incision from the forehead to the back of the skull. Use a sterile cotton-tipped applicator to stabilize the skin to facilitate the incision. Gently push scalp skin to the sides so that an area of the skull is exposed from the bregma, which is located near the middle of the skull, to the eyes. The bregma is a juncture in the cranial plates, where the coronal suture intersects perpendicularly to the sagittal suture.
6. Stabilize a 26-gauge needle attached to a Neuros™ 10 μl syringe filled with 5 μl of cell suspension, containing ~1×10^6 Ben-Men-1-LucB cells, in the stereotactic device and position it above the bregma. An OPMI Pro Magis surgical microscope is helpful in visualizing the bregma.
7. After the needle of the syringe is positioned directly above the bregma, set each of the stereotactic coordinates to zero. Then, using the stereotactic axes, move the syringe 1.5 mm anterior to the bregma and 1.5 mm lateral to the right of the bregma. Make a small burr hole at this location using a high-speed micro drill.
8. Once the drill has completely penetrated the skull so that the brain is exposed, lower the syringe until the tip of the needle is at the surface of the brain. Prior to inserting the needle into the brain, set the coordinate of the *Z*-axis to zero, and confirm coordinates for the *X*- and *Y*-axes (1.5 mm anterior and 1.5 mm lateral to the right of the bregma).

9. Once positioned, lower the needle slowly 4.5 mm into the brain to the skull base (*see* **Note 12**).
10. Using an automatic injector, inject tumor cells into the skull base at a rate of 1.5 ml/min. After the cells have been completely dispensed, maintain the needle in place for one minute to permit the injected cells to settle, followed by slowly withdrawing the needle from the brain.
11. Using a pair of forceps, close the surgical incision with Vetbond tissue adhesive.
12. As in Subheading 3.3, **step 7**, inject a dose of buprenorphine (0.05 mg/kg) subcutaneously near the surgical site as an analgesic. Remove the mouse from the stereotactic device and place on a thermo-controlled recovery pad until full recovery.

3.5 Monitoring Growth of Schwannoma Allografts and Meningioma Xenografts by BLI

1. BLI is used to assess successful tumor engraftment and growth. Prior to imaging, inject mice, implanted with Sch10545-Luc or Ben-Men-1-LucB cells, intraperitoneally with 150 mg/kg of D-luciferin (*see* **Note 11**).
2. As in Subheadings 3.3 and 3.4, **steps 3**, anesthetize mice using 5 % isoflurane in oxygen. Place the anesthesized mouse in the IVIS Spectrum Preclinical In Vivo Imaging System and position the nose in the nose cone for isoflurane gas administration during imaging.
3. Capture bioluminescent images of tumor-bearing mice at the peak time of luciferase activity following injection of D-luciferin (*see* **Note 13**).
4. Using BLI, tumor growth is measured noninvasively over time. The intensity of the BL signal correlates with changes in tumor size and is measured in each mouse using region-of-interest analysis in the LivingImage software (*see* **Note 14**). To determine tumor establishment and growth prior to treatment, at least two bioluminescent images should exhibit robust and increasing signals. We have found that tumor growth in the Sch10545-Luc schwannoma allograft model is effectively detected over one-week time intervals, whereas growth in the Ben-Men-1-LucB meningioma xenograft model is best observed over 1-month intervals.
5. To assess the efficacy of a particular therapeutic agent, compare the intensity of the BL signal (*see* **Note 15**) and its changes over time among animals treated with a therapeutic agent and untreated controls (*see* **Note 16**). Treatment responses can be confirmed by small-animal MRI [12, 19].

4 Notes

1. Antibiotics, such as penicillin and streptomycin, are used to reduce contamination, particularly during preparation of primary cultures of VS and meningioma cells. The details regarding preparation of these primary tumor cell cultures have been described previously [16]. However, we try to avoid using antibiotics, whenever it is possible, e.g., culturing established cell lines.
2. To generate an *Nf2*-deficient schwannoma cell line, schwannoma cells from $Nf2^{P0}$ mice were cultured for more than 25 passages and subcloned. We isolated a clone, designated Sch10545, which exhibits continuous growth. Loss of the *Nf2* gene in these cells was confirmed by PCR genotyping and Western blotting [16, 17]. Interestingly, these cells are no longer dependent on HRG and can grow in medium supplemented with 10 % FBS.
3. The benign human meningioma cell line Ben-Men-1 was established from a grade I meningioma by telomerase immortalization [18]. By Western blotting and DNA sequencing, we previously showed that Ben-Men-1 cells are Merlin-deficient [19].
4. Lentiviral vectors, such as Lenti-CMV-Luc, are considered Biosafety Level 2 (BSL-2) agents. Although they are replication-deficient, all handling and storage of lentiviral vectors and disposal of contaminated waste must be conducted according to institutional rules and regulations and NIH guidelines. Lentiviral vectors should be aliquoted in small amounts and stored at −80 °C. Repeated freeze–thawing will decrease the viral titer.
5. Other optimized firefly luciferase expression vectors [20–22] can be used, as well as luciferase-expressing vectors from other species [23, 24].
6. The optimal MOI is dependent on the target cell type and should be titrated to enhance viral gene delivery. Infection time may be decreased, or purified viral particles are used if viral toxicity is observed in the cell line of interest, particularly when using viral supernatant.
7. Polybrene is a cation polymer that can enhance retroviral or lentiviral transduction efficiency, by neutralizing the charge repulsion between viral particles and sialic acid moieties on the cell surface [25]. However, polybrene may be toxic to some cell lines, calling for a shorter incubation time. Alternatively, protamine sulfate [26] or other reagent systems, such as ViraDuctin™ or Sigma's ExpressMag bead system, are used to increase the efficiency of viral infection.

8. The optimal concentration of puromycin for the selection of puromycin-resistant clones should be determined in advance. For this purpose, we usually use the minimal concentration of puromycin that is sufficient to kill all non-transduced cells. Puromycin should be added 24 h after infection to allow for sufficient expression of the puromycin-resistant gene.
9. Different sizes of cloning cylinders can be purchased and used to isolate individual puromycin-resistant colonies. Alternatively, dilution cloning can be performed using 96-well plates. Also, it is possible to plate cells at a low density and directly select individual puromycin-resistant colonies in 96-well plates 24 h or more after lentiviral transduction.
10. For engraftment of schwannoma and meningioma cells, we routinely use the *scid* strain of immunodeficient mice, which carry the defective DNA-activated protein kinase Prkdc, important for the rearrangement of the immunoglobulin and T-cell receptor genes [27]. Other immunodeficient mouse strains, such as nonobese diabetic (NOD)-*scid β2m*null and NOD-*scid IL2Rγnull* (also called NSG or NOD *scid* gamma), may be considered as they give rise to more rapid tumor engraftment in some tumor models [28, 29]. Due to the *β2m*null mutation, NOD-*scid β2m*null mice are deficient in MHC class I expression, and their natural killer (NK) cells are unable to kill susceptible targets upon activation [30]. The NOD-*scid IL2R*γnull strain harbors a mutation in *IL2Rγ*, which encodes the cytokine-receptor γ-chain shared by IL-2, IL-4, IL-7, IL-9, IL-15, and IL-21 receptors, and exhibits impaired NK cell development [31].
11. It can be helpful to stabilize mouse legs by taping their toes to the platform during surgery. The sciatic nerve can be accessed from either the dorsal or ventral sides of the mouse. It is preferable to graft only one sciatic nerve in each mouse as grafting both nerves will lead to impaired function of both hind legs due to tumor growth, resulting in early removal of mice from the study.
12. The depth to which the needle needs to be lowered to reach the skull base may vary slightly, depending on the age of the mice. Using 8-to-12-week-old mice, a depth of 4.5 mm is a useful guideline for skull base injection.
13. The sensitivity with which tumors are measured depends on the level of luciferase expression in the clones. Stronger luciferase activity yields a strong BL signal for a smaller number of cells, enabling the detection of fewer cells in a tumor. D-luciferin is commonly used for BLI in mice. Recently, a synthetic luciferin, the cyclic alkylaminoluciferin (CycLuc1), was shown to exhibit improved light output and to enhance BL detection in deep tissues, such as the brain [32].

14. The kinetics of luciferin circulation and uptake by tumor cells may vary in different models. To facilitate accurate quantitation of tumor growth, measurements are performed when luciferase activity is highest. This peak time is determined by measuring in vivo luciferase activity at various time intervals after D-luciferin injection. All subsequent bioluminescence measurements should be performed at this time interval.
15. As a sensitive and efficient way to noninvasively monitor tumor growth, BLI facilitates longitudinal studies, particularly for benign tumors [19]. Studies suggest that BL signals detected in luciferase-expressing tumors correlate with tumor size detected by MRI. BLI and MRI complement each other well by quantifying viable tumor cells and measuring the volume of the tumor mass by clinical standards, respectively.
16. Recently, interest is gaining in orthotopic patient-derived xenografts (PDX) as preclinical models for drug screening and development [33]. Loss of the *NF2* gene product Merlin leads to deregulation of multiple signaling pathways, such as the mitogen-activated protein kinase (MAPK) and PI3K/AKT/mTOR pathways, which may serve as viable therapeutic targets [1]. Study of these pathways has led to the initiation of several clinical trials. These schwannoma and meningioma animal models should enhance evaluation of additional novel therapeutic compounds.

Acknowledgments

The authors would like to thank Dr. D. Bradley Welling for discussion. This work was supported by grants from the Department of Defense, Children's Tumor Foundation, Advocure NF2, Meningioma Mommas, and the Galloway Family.

References

1. Yates C, Welling DB, Chang L-S (2011) Research advances in therapeutics for neurofibromatosis type 2-associated vestibular schwannomas. In: Cunha KS, Geller M (eds) Advances in neurofibromatosis research. Nova Science Publishers, Inc., Hauppauge, NY
2. Wiemels J, Wrensch M, Claus EB (2010) Epidemiology and etiology of meningioma. J Neurooncol 99:307–314
3. Baser ME, Friedman JM, Aeschliman D, Joe H, Wallace AJ, Ramsden RT, Evans DG (2002) Predictors of the risk of mortality in neurofibromatosis 2. Am J Hum Genet 71:715–723
4. Goutagny S, Kalamarides M (2010) Meningiomas and neurofibromatosis. J Neurooncol 99:341–347
5. Rouleau GA, Merel P, Lutchman M et al (1993) Alteration in a new gene encoding a putative membrane-organising protein causes neurofibromatosis type 2. Nature 363:515–521
6. Trofatter JA, MacCollin MM, Rutter JL et al (1993) A novel Moesin-, Exrin-, Radixin-like gene is a candidate for the neurofibromatosis 2 tumor-suppressor. Cell 72:791–800
7. Bianchi AB, Hara T, Ramesh V et al (1994) Mutations in transcript isoforms of the neurofibromatosis 2 gene in multiple human tumour types. Nat Genet 6:185–192
8. Bianchi AB, Mitsunnaga SI, Cheng JQ, Klein WM, Jhanwar SC, Seizinger B, Kley N, Klein-Szanto AJ, Testa JR (1995) High frequency of inactivating mutations in the neurofibromatosis

type 2 gene (*NF2*) in primary malignant mesotheliomas. Proc Natl Acad Sci U S A 92:10854–10858

9. Giovannini M, Robanus-Maandag E, van der Valk M, Niwa-Kawakita M et al (2000) Conditional biallelic Nf2 mutation in the mouse promotes manifestations of human neurofibromatosis type 2. Genes Dev 14:1617–1630
10. Kalamarides M, Stemmer-Rachamimov AO, Niwa-Kawakita M, Chareyre F, Taranchon E, Han ZY, Martinelli C, Lusis EA, Hegedus B, Gutmann DH, Giovannini M (2011) Identification of a progenitor cell of origin capable of generating diverse meningioma histological subtypes. Oncogene 30:2333–2344
11. Gehlhausen JR, Park SJ, Hickox AE et al (2015) A murine model of neurofibromatosis type 2 that accurately phenocopies human schwannoma formation. Hum Mol Genet 24:1–8
12. Chang L-S, Jacob A, Lorenz M, Rock J et al (2006) Growth of benign and malignant schwannoma xenografts in severe combined immunodeficiency mice. Laryngoscope 116:2018–2026
13. Neff BA, Voss SG, Allen C, Schroeder MA, Driscoll CL, Link MJ, Galanis E, Sarkaria JN (2009) Bioluminescent imaging of intracranial vestibular schwannoma xenografts in NOD/SCID mice. Otol Neurotol 30:105–111
14. Lin AL, Gutmann DH (2013) Advances in the treatment of neurofibromatosis-associated tumours. Nat Rev Clin Oncol 10:616–624
15. Wang Y, Tseng JC, Sun Y, Beck AH, Kung AL (2015) Noninvasive imaging of tumor burden and molecular pathways in mouse models of cancer. Cold Spring Harb Protoc 2015:135–144
16. Chang L-S, Welling DB (2009) Molecular biology of vestibular schwannomas. In: Sokolowski B (ed) Auditory/vestibular research, The Humana Press, Totowa, NJ, Methods Mol Biol 493:163–177
17. Spear SA, Burns SS, Oblinger JL, Ren Y, Pan L, Kinghorn AD, Welling DB, Chang L-S (2013) Natural compounds as potential treatments of *NF2*-deficient schwannoma and meningioma: cucurbitacin D and goyazensolide. Otol Neurotol 34:1519–1527
18. Püttmann S, Senner V, Braune V, Hillmann B, Exeler R, Rickert C et al (2005) Establishment of a benign meningioma cell line by hTERT-mediated immortalization. Lab Invest 85: 1163–1171
19. Burns SS, Akhmametyeva EA, Oblinger JL, Bush ML, Huang J, Senner V, Chen C-S, Jacob A, Welling DB, Chang L-S (2013) AR-42, a histone deacetylase inhibitor, differentially affects cell-cycle progression of meningeal and meningioma cells and potently inhibits *NF2*-meningioma growth. Cancer Res 73:792–803
20. Rabinovich BA, Ye Y, Etto T, Chen JQ, Levitsky HI, Overwijk WW, Cooper LJ, Gelovani J, Hwu P (2008) Visualizing fewer than 10 mouse T cells with an enhanced firefly luciferase in immunocompetent mouse models of cancer. Proc Natl Acad Sci U S A 105:14342–14346
21. Kim JB, Urban K, Cochran E, Lee S, Ang A, Rice B, Bata A, Campbell K, Coffee R, Gorodinsky A, Lu Z, Zhou H, Kishimoto TK, Lassota P (2010) Non-invasive detection of a small number of bioluminescent cancer cells *in vivo*. PLoS One 5:e9364
22. Harwood KR, Mofford DM, Reddy GR, Miller SC (2011) Identification of mutant firefly luciferases that efficiently utilize aminoluciferins. Chem Biol 18:1649–1657
23. Prescher JA, Contag CH (2010) Guided by the light: visualizing biomolecular processes in living animals with bioluminescence. Curr Opin Chem Biol 14:80–89
24. Mezzanotte L, Fazzina R, Michelini E, Tonelli R, Pession A, Branchini B, Roda A (2010) In vivo bioluminescence imaging of murine xenograft cancer models with a red-shifted thermostable luciferase. Mol Imaging Biol 12: 406–414
25. Davis HE, Morgan JR, Yarmush ML (2002) Polybrene increases retrovirus gene transfer efficiency by enhancing receptor-independent virus adsorption on target cell membranes. Biophys Chem 97:159–172
26. Cornetta K, Anderson WF (1989) Protamine sulfate as an effective alternative to polybrene in retroviral-mediated gene-transfer: implications for human gene therapy. J Virol Methods 23:187–194
27. Shultz LD, Ishikawa F, Greiner DL (2007) Humanized mice in translational biomedical research. Nat Rev Immunol 7:118–130
28. Ito M, Hiramatsu H, Kobayashi K et al (2002) NOD/SCID/γcnull mouse: an excellent recipient mouse model for engraftment of human cells. Blood 100:3175–3182
29. Carreno BM, Garbow JR, Kolar GR, Jackson EN, Engelbach JA, Becker-Hapak M, Carayannopoulos LN, Piwnica-Worms D, Linette GP (2009) Immunodeficient mouse strains display marked variability in growth of human melanoma lung metastases. Clin Cancer Res 15:3277–3286
30. Kim S, Poursine-Laurent J, Truscott SM et al (2005) Licensing of natural killer cells by host

major histocompatibility complex class I molecules. Nature 436:709–713

31. Shultz LD, Lyons BL, Burzenski LM, Gott B, Chen X, Chaleff S et al (2005) Human lymphoid and myeloid cell development in NOD/LtSz-scid IL2R gamma null mice engrafted with mobilized human hemopoietic stem cells. J Immunol 174:6477–6489
32. Evans MS, Chaurette JP, Adams ST Jr, Reddy GR, Paley MA, Aronin N, Prescher JA, Miller SC (2014) A synthetic luciferin improves bioluminescence imaging in live mice. Nat Methods 11:393–395
33. Wilding JL, Bodmer WF (2014) Cancer cell lines for drug discovery and development. Cancer Res 74:2377–2384

www.impactjournals.com/oncotarget/ Oncotarget, 2017, Vol. 8, (No. 19), pp: 31666-31681

Research Paper

Ponatinib promotes a G_1 cell-cycle arrest of merlin/NF2-deficient human schwann cells

Alejandra M. Petrilli[1], Jeanine Garcia[1], Marga Bott[1], Stephani Klingeman Plati[1], Christine T. Dinh[2], Olena R. Bracho[2], Denise Yan[2], Bing Zou[2], Rahul Mittal[2], Fred F. Telischi[2], Xue-Zhong Liu[2], Long-Sheng Chang[3], D. Bradley Welling[3,4], Alicja J. Copik[1] and Cristina Fernández-Valle[1]

[1]Burnett School of Biomedical Sciences, College of Medicine, University of Central Florida, Lake Nona-Orlando, FL 32827, USA

[2]University of Miami Miller School of Medicine, Department of Otolaryngology, Miami, FL 33136, USA

[3]Center for Childhood Cancer and Blood Diseases, The Research Institute at Nationwide Children's Hospital and Department of Pediatrics, The Ohio State University College of Medicine, Columbus, OH 43205, USA

[4]Current Affiliation: Department of Otolaryngology, Massachusetts Eye and Ear Infirmary, Massachusetts General Hospital and Harvard University, Boston, MA 02114, USA

Correspondence to: *Cristina Fernández-Valle,* ***email:*** *cfv@ucf.edu*

Keywords: *neurofibromatosis type 2, schwannoma, PDGFR, SRC, STAT3*

Received: *August 17, 2016* ***Accepted:*** *February 20, 2017* ***Published:*** *March 06, 2017*

ABSTRACT

Neurofibromatosis type 2 (NF2) is a genetic syndrome that predisposes individuals to multiple benign tumors of the central and peripheral nervous systems, including vestibular schwannomas. Currently, there are no FDA approved drug therapies for NF2. Loss of function of merlin encoded by the *NF2* tumor suppressor gene leads to activation of multiple mitogenic signaling cascades, including platelet-derived growth factor receptor (PDGFR) and SRC in Schwann cells. The goal of this study was to determine whether ponatinib, an FDA-approved ABL/SRC inhibitor, reduced proliferation and/or survival of merlin-deficient human Schwann cells (HSC). Merlin-deficient HSC had higher levels of phosphorylated PDGFRα/β, and SRC than merlin-expressing HSC. A similar phosphorylation pattern was observed in phospho-protein arrays of human vestibular schwannoma samples compared to normal HSC. Ponatinib reduced merlin-deficient HSC viability in a dose-dependent manner by decreasing phosphorylation of PDGFRα/β, AKT, p70S6K, MEK1/2, ERK1/2 and STAT3. These changes were associated with decreased cyclin D1 and increased $p27^{Kip1}$ levels, leading to a G_1 cell-cycle arrest as assessed by Western blotting and flow cytometry. Ponatinib did not modulate ABL, SRC, focal adhesion kinase (FAK), or paxillin phosphorylation levels. These results suggest that ponatinib is a potential therapeutic agent for NF2-associated schwannomas and warrants further *in vivo* investigation.

INTRODUCTION

Neurofibromatosis type 2 (NF2) is a non-malignant tumor disorder affecting the peripheral and central nervous systems. Although bilateral vestibular schwannomas (VS) are a diagnostic hallmark of the disorder, NF2 patients typically develop multiple meningiomas, ependymomas and other schwannomas as well. VS lead to deafness, tinnitus, imbalance and can cause life-threatening brainstem compression [1]. NF2 is caused by mutations in the *NF2* gene that encodes the tumor suppressor protein known as merlin or schwannomin [2, 3]. Merlin belongs to the Band 4.1 family of proteins that link the actin cytoskeleton to membrane receptors and transporters. Merlin modulates the activity of multiple signaling pathways that control cell size, morphology, cell adhesion, proliferation, and survival. These include receptor tyrosine kinase (RTK; e.g. ErbB2/3, PDGFR, EGFR, HGFR), small GTPases, FAK/SRC, the mammalian target of rapamycin (mTOR)/PI3K/AKT, and Hippo pathways [4]. Currently, surgery and radiation are the mainstream treatment options for NF2-associated tumors. Depending on the tumor

size and location, there are significant adverse effects associated with their removal. While an understanding of the biological functions of merlin is progressing, well-defined druggable molecular targets have yet to emerge. Increasingly, patients are treated off-label with the anti-angiogenic agent bevacizumab that also reduces edema in schwannomas without affecting the tumor cells. Dosing regimens are being optimized to reduce associated kidney toxicity observed with prolonged bevacizumab treatment [1, 5]. However, to date there are no FDA-approved therapies that target schwannoma cells directly and reduce morbidity and mortality of NF2 patients [1, 6].

Because of the slow-growing and benign nature of NF2 schwannomas, conventional chemotherapeutic agents are unsuccessful. Several RTK inhibitors have been investigated in preclinical studies and clinical trials with limited patient response. These include lapatinib (an EGFR/ErbB2 inhibitor; NCT00973739, NCT00863122), nilotinib (a PDGFR and c-kit inhibitor; NCT01201538), sorafenib (a VEGFR-2, PDFGRβ, and c-kit inhibitor), and axitinib (a VEGFR, c-kit, and PDGFRβ inhibitor; NCT02129647) [1, 7]. We selected ponatinib for evaluation because it is an FDA-approved drug that inhibits a relevant RTK, the PDGFR, and a downstream effector common to several *NF2* activated pathways, the non-receptor tyrosine kinase SRC. PDGFR and SRC signaling regulate cell survival, proliferation, migration and angiogenesis in many cell types [8, 9]. PDGFR is over-expressed and activated in VS and primary human schwannoma cells, consistent with merlin's role in downregulating surface levels of growth factor receptors [10-13]. In HEI-193 schwannoma cells, merlin overexpression inhibits cell proliferation by promoting PDGFR internalization and degradation [14]. There is evidence that SRC activity is deregulated in cells with loss of merlin function and thus is a candidate for therapeutic targeting. In human schwannoma cells, SRC activity is increased compared to normal Schwann cells, and in mouse glia cells, merlin inhibits proliferation by modulating SRC activity [15, 16]. Lastly, primary human schwannoma cells treated with the SRC inhibitor SU6656 exhibit decreased transcription of proliferation-associated genes [17]. Thus, an inhibitor that targets both PDGFR and SRC might have therapeutic value for NF2-associated tumors.

Ponatinib (AP24534, brand name: Iclusig®) is a third generation type IIA inhibitor of ABL/SRC tyrosine kinase (TK). It is orally active and initially received accelerated approval in 2012 for adult patients with chronic myeloid leukemia (CML) and Philadelphia chromosome-positive acute lymphoblastic leukemia (Ph+ ALL) that are T315I-positive and are not candidates for other TK inhibitors. Ponatinib binds the inactive, DFG-out (aspartic acid, phenylalanine and glycine) ABL/SRC conformation [18, 19]. In a cell-free kinase screen, ponatinib inhibited SRC with IC_{50} of 5.4nM and PDGFRα and PDGFRβ with IC_{50} of 1.1nM and 7.7nM, respectively [19].

In this study, we measured the ability of ponatinib to decrease proliferation and survival of merlin-deficient HSC and vestibular schwannoma cells with *NF2* mutations. We found that ponatinib caused a G_1 cell-cycle arrest and mapped the regulatory signaling cascades modulated by the inhibitor. Our findings support further *in vivo* evaluation of ponatinib as a candidate drug for NF2 schwannomas.

RESULTS

Ponatinib decreases viability of merlin-deficient HSC and vestibular schwannoma (VS) cells

To create a suitable cell line for drug discovery studies, we first authenticated primary HSC based on their expression of human nuclear antigen and Schwann cell markers, S100, PLP, and O4 (Figure 1A). We then used lentiviral delivery of NF2-shRNA to reduce expression of merlin in the primary HSC. Merlin levels were stably reduced to nearly undetectable levels in the transduced cells compared to the parental HSC (Figure 1B, C). The merlin-deficient HSC did not contact inhibit but did not form aggregates and grows in multiple layers; many of these merlin-deficient HSC maintained an elongated morphology when cultured in the presence of serum and mitogens (Supplementary Figure 1AB). We measured basal levels of PDGFRα/β and SRC phosphorylation in primary HSC prior to and following knockdown of merlin. We found that depletion of merlin expression was associated with increased levels of p-PDGFRα/β and p-SRC compared to the parental HSC (Figure 1B). This finding agrees with previous reports of increased activation of the PDGFR and SRC pathways in human schwannomas compared to normal human nerve [10, 20, 21].

We screened the ability of ponatinib to reduce viability of multiple control and merlin-deficient HSC lines. As controls, we tested the parental wild-type HSC (HSC-WT), HSC expressing a scrambled shRNA construct (HSC-SCR), HSC expressing a Turbo-GFP shRNA (HSC-GFP), and merlin-deficient HSC lines (MD-HSC) expressing shRNA sequences that target the human *NF2* gene, (MD-HSC #45, #74 #75 and #77). All control HSC expressed merlin, whereas the HSCs transduced with shRNA constructs targeting the *NF2* gene had nearly undetectable merlin levels (Figure 1D). We performed 48 hour dose-response viability assays on the seven HSC lines in complete growth medium containing serum and growth factors. The results indicated that ponatinib reduced viability of all of the cell lines in a dose-dependent manner (Figure 1E). Under the conditions tested, ponatinib was not selective for MD-HSC over scrambled, GFP or untransduced HSC (IC_{50} HSC-SCR= 3.3μM, HSC-GFP=2.4 μM, HSC-WT= 2.3 μM, MD-HSC#45= 2.2 μM, MD-HSC#74= 3.3 μM, MD-HSC#75= 1.9 μM and MD-HSC#77=3.7 μM). The average maximal response at 10μM was a 71% decrease in cell viability. However, when control merlin-expressing cell

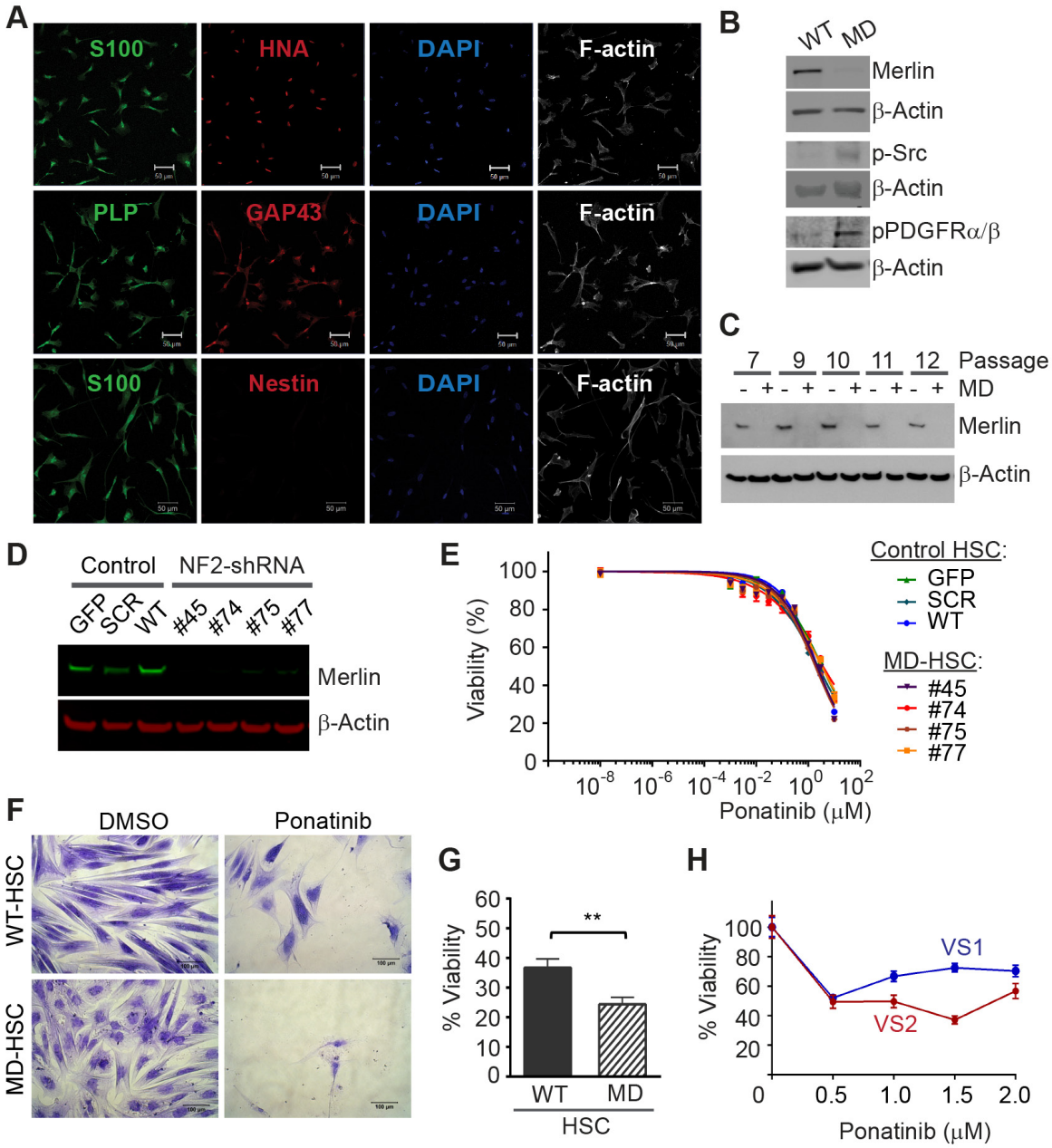

Figure 1: Ponatinib decreases HSC viability. (A) Characterization of primary HSC. Confocal Images of HSC expressing human and SC linage markers: human nuclear antigen (HNA, red), S100 (green), GAP43 (red), proteolipid protein (PLP, green), negative nestin (red), DAPI stained nuclei (blue) and F-actin was visualized with phaloidin-Alexa633 (white). Scale bar: 50μm. **(B)** Representative Western blots of primary HSC and merlin-deficient HSC (MD-HSC) lysates, merlin silencing increased levels of phosphorylated SRC and PDGFRα/β. **(C)** Western blotting for merlin and β-actin in control HSC and merlin deficient cells at increasing cell passages. **(D)** Western blot for merlin and β-actin in three control HSC lines and four merlin-deficient (knock-down) HSC lines. **(E)** Ponatinib dose-response CellTiter-Fluor viability assay. Control HSC lines: SCR-HSC, GFP-HSC and WT-HSC and merlin-deficient HSC: #45, 74, 75, 77 were treated with increasing concentrations of ponatinib in constant 0.1% DMSO or vehicle alone for 48h. Viability is presented as a % of the DMSO control. Graph represents the mean ± SEM of three independent experiments. **(F-G)** WT-HSC and MD-HSC (#45) were maintained in serum free medium for 5-10 days and then treated with 0.25μM ponatinib for one week. Relative cell numbers was assessed using a crystal violet assay: **(F)** Representative 20X phase contrast images of cells. Scale bar= 100μm. **(G)** Cell viability calculated as a % of their respective DMSO control. Graph represent mean ± SEM of three independent experiments (** $p<0.01$, unpaired *t*-test, two tailed). **(H)** Viability of primary human VS cells treated for 48h with increasing ponatinib concentrations. Relative cell viability was assessed using a crystal violet assay and presented as % viability normalized to DMSO group. Plot of mean ± SEM of 6 replicates. VS1 (heterozygous deletion of 23 nucleotides in exon 8 of the *NF2* gene, non-irradiated, passage 2); VS2 (heterozygous missense c.1460T>A and p. I487N in exon 14 of the *NF2* gene, non-irradiated, passage 2).

line (HSC-WT) and merlin-deficient HSC (MD-HSC#45) were cultured in the absence of serum and mitogens, merlin-deficient HSC were significantly more sensitive to 0.25 μM ponatinib than the merlin-expressing HSC (Figure 1F,G).

We tested ponatinib's effect on cultured human vestibular schwannoma cells with *NF2* mutations. We assessed relative cell viability using a crystal violet assay following 48 hour incubation with ponatinib. Cell viability was reduced by approximately 40% at 2μM in VS1 and VS2 compared to DMSO-treated cells in agreement with the IC_{50} obtained with our MD-HSC lines. (Figure 1H).

Ponatinib decreases viability of merlin-deficient HSC independent of the SRC/FAK/paxillin pathway

Ponatinib did not reduce net levels of ABL phosphorylation in merlin-deficient HSC (Figure 2A). Ponatinib induced a dose-dependent increase in the total SRC protein level but did not alter the levels of the other SRC family members, FYN and YES, that play important roles in SC biology as well (Figure 2B) [22, 23]. We found a slight increase in SRC-Tyr416 phosphorylation in merlin-deficient HSC treated with 0.3 to 3μM (with a peak at 1μM). The phosphorylation pattern, however, did not coincide with the increase in the SRC protein levels (Figure 2B).

Key effectors transducing extracellular matrix adhesion and growth factor-dependent stimuli in Schwann cells are the SRC substrates, FAK and paxillin, a focal adhesion-associated adaptor [24]. FAK is a key mediator of extracellular matrix-integrin and RTK signaling that is upregulated in schwannomas [10]. Upon FAK autophosphorylation at Tyr397, SRC binds the phosphorylated residue and phosphorylates FAK on Tyr576 and Tyr577, resulting in stabilizing the activation loop of FAK in the active conformation and its binding to substrates,

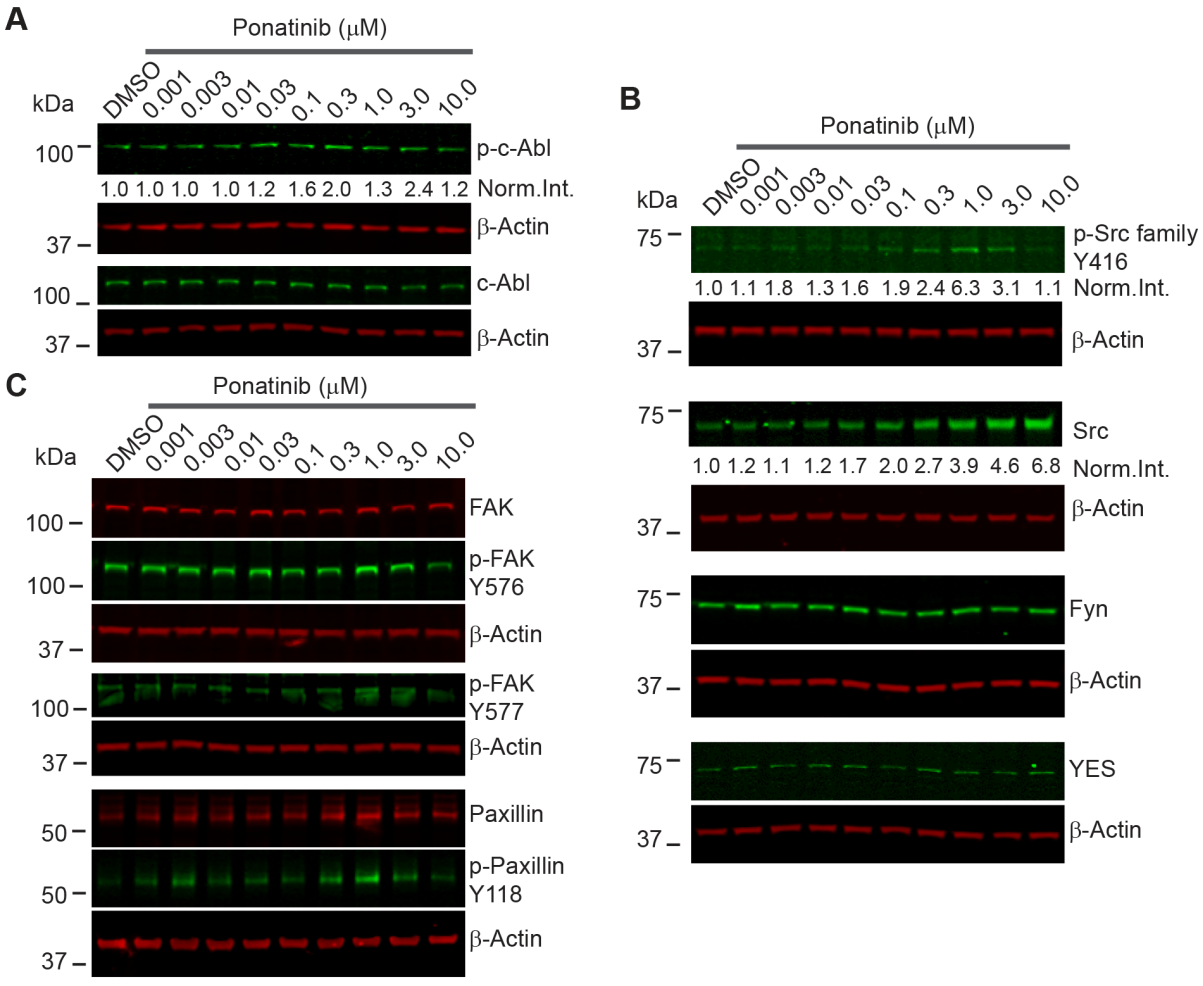

Figure 2: Ponatinib decreased merlin-deficient HSC viability independent of ABL/SRC/FAK pathway inhibition. Representative ponatinib dose-response Western blots (n=3). MD- HSC#45 plated in 12-well plates were treated with increasing concentrations of ponatinib for 2h as indicated. Cells were harvested, lysed, resolved by SDS-PAGE and blotted for: **(A)** p-ABL-Tyr452, c-ABL and β-actin as a loading control; **(B)** p-SRC-Tyr416 and total SRC, FYN, YES, p-FAK-Tyr576, p-FAK-Tyr577, total FAK, p-Paxillin-Tyr118, and total paxillin. The β-actin levels were used as loading controls.

thereby providing FAK with maximal activity [25]. In turn, FAK either directly or via SRC, phosphorylates paxillin at Tyr118 [26]. We therefore assessed FAK and paxillin phosphorylation in merlin-deficient HSC treated for 2h with increasing ponatinib concentrations. Western blot analysis showed that ponatinib did not reduce FAK-Tyr576 or Tyr577 or paxillin-Tyr118 phosphorylation similar to the SRC-Tyr416 phosphorylation pattern (Figure 2C and Supplementary Figure 2). Together the results demonstrate that the ABL, SRC, FAK and paxillin pathways are not inhibited by ponatinib in merlin-deficient HSC.

Ponatinib decreases activation of the PDGFRα/β, PI3K, MEK1/2, ERK1/2 and STAT3 signaling pathways

To identify the signaling pathways modulated by ponatinib, we conducted a series of Western blots of merlin-deficient HSC treated for 2 hours with increasing concentrations of ponatinib. We found that ponatinib reduced phosphorylation of PDGFRα/β at Tyr849/Tyr857, the autophosphorylation sites in the activation loop of these kinases, in a dose-dependent manner without altering the PDGFRα/β protein levels (Figure 3). In addition, ponatinib reduced phosphorylation of three additional tyrosine residues in PDGFRβ at positions 740, 771 and 1021 (Figure 3). Phosphorylation of these residues increases affinity for binding and activating PI3K, SRC, the GTPase Activator of Ras (GAP), GRB2, and PLCγ [27]. When cells are stimulated with growth factors, AKT (also known as protein kinase B) and p70 S6 kinase are activated in a phosphatidylinositol 3-kinase (PI3K)-dependent pathway. Thr308 in the AKT activation loop and Thr229 in the p70S6 kinase catalytic domain are phosphorylated by 3-phosphoinositide-dependent protein kinase-1 (PDK1) *in vivo* and *in vitro* [28, 29]. Therefore to probe activity of the PI3K pathway in ponatinib-treated cells, we assessed AKT-Thr308 phosphorylation and p70S6 kinase-Thr229

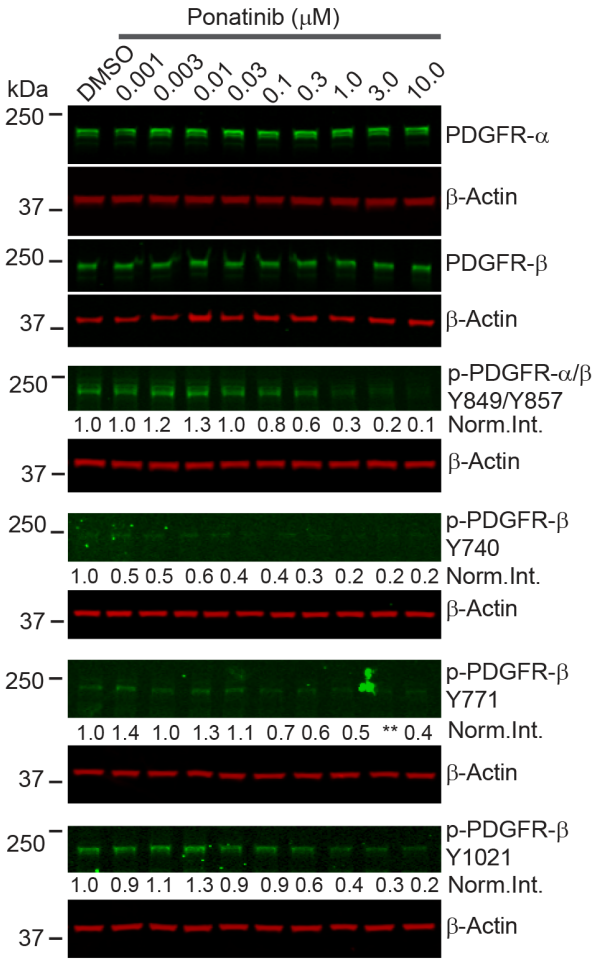

Figure 3: Ponatinib inhibited PDGFRα/β phosphorylation in merlin-deficient HSC. Representative ponatinib dose-response Western blots (n=3). MD-HSC#45 plated in 12-well plates were treated with increasing concentrations of ponatinib for 2h as indicated. Cells were harvested, lysed, resolved by SDS-PAGE and blotted for p-PDGFRα/β-Tyr849/Tyr857, p-PDGFRβ-Tyr740, p-PDGFRβ-Tyr771, p-PDGFRβ-Tyr1021 and total PDGFRα and PDGFRβ. The β-actin levels were used as loading controls.

phosphorylation by Western blots. We found that both AKT-Thr308 and p70S6 kinase-Thr229 underwent a dose-dependent decrease in phosphorylation (Figure 4A,B).

Previous studies demonstrated that overexpression and activation of PDGFRβ strongly activates MEK1/2 and ERK1/2 in human schwannoma cells leading to enhanced proliferation [10]. We assessed the phosphorylated MEK1/2 and ERK1/2 levels in merlin-deficient HSC after ponatinib treatment. We found that ponatinib treatment was associated with a dose-dependent decrease in MEK1/2-Ser217/Ser221 and ERK1/2-Thr202/Tyr204 phosphorylation in merlin-deficient HSC (Figure 4C).

Although net inhibition of SRC phosphorylation was not observed, ligand binding to PDGFR promotes receptor binding to SRC and recruitment of STAT3, followed by Tyr705 auto-phosphorylation of STAT3 and its dimerization and translocation into the nucleus to directly drive gene expression needed for cell proliferation [30-32]. Western blot analysis showed that ponatinib decreased STAT3 phosphorylation in a dose-dependent manner in merlin-deficient HSC (Figure 4D).

Lastly, to further evaluate the contribution of PI3K/AKT, MEK, or STAT3 inhibition downstream to PDGFR responsible for ponatinib's effect, we individually inhibited AKT with perifosine/KRX-0401, MEK with selumetinib/AZD6244, and STAT3 with S3I-201/NSC-74859 and compared the results to ponatinib's effects on cell viability. MEK, AKT or STAT3 inhibition alone only partially decreased merlin-deficient HSC viability. Inhibition of STAT3 with S3I-201 was the least effective,

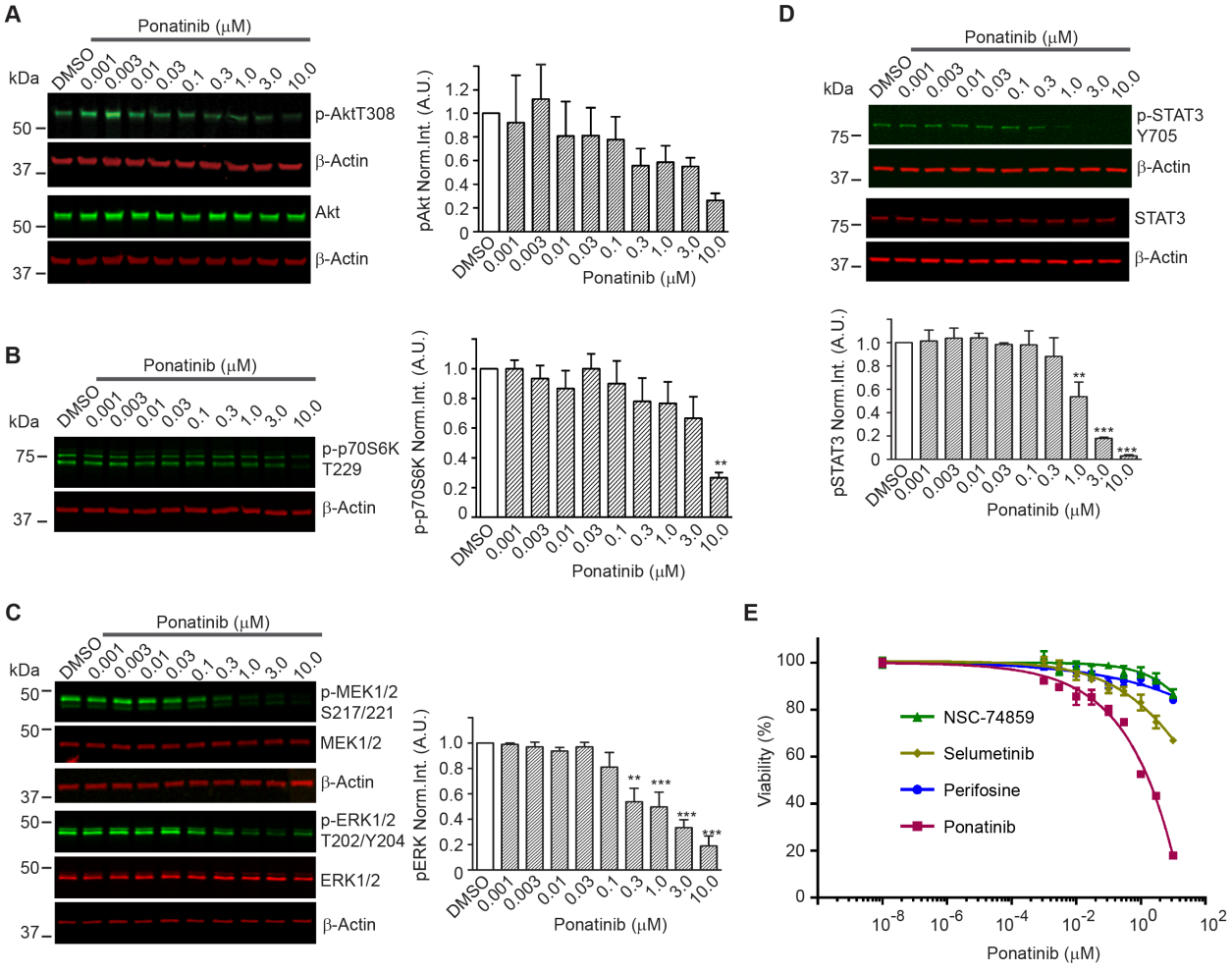

Figure 4: Downstream signaling pathways inhibited by ponatinib in merlin-deficient HSC. Western blots of extracts prepared from merlin-deficient HSC#45 treated with increasing ponatinib concentrations. Quantitation was done by fluorescence intensity analysis, normalized to β-actin, and plotted as mean ± SEM (n=3). One-way analysis of variance and Dunnett's multiple comparison post-test were used for statistical analysis (* p<0.1; ** p<0.01 and *** p<0.001). Representative Western blots of dose response experiments at 2h for: **(A)** p-AKT-Thr308 and AKT; **(B)** p-p70S6K-Thr229; **(C)** MEK1/2, p-MEK1/2-Ser217/Ser221, ERK1/2, and p-ERK1/2-Thr202/Tyr204; **(D)** p-STAT3-Tyr705, and total STAT3. (**E**) Ponatinib dose-responseCellTiter-Fluor viability assay. MD- HSC#45 were treated with semi-log serial dilutions of ponatinib, NSC-74859, selumetinib, perifosine in 0.1% DMSO for 48h, or vehicle alone. Viability is presented as % of the DMSO control. Graph represents the mean ± SEM of three independent experiments.

and although selumetinib was more efficacious than perifosine and S3I-201, none of individual inhibitors even at the highest concentration tested (10 μM) matched ponatinib's efficacy (Figure 4E). These results suggest that simultaneous inhibition of these three pathways occurs in response to ponatinib and similarly contributes to the loss of viability of merlin-deficient HSC.

Ponatinib arrests merlin-deficient HSC in G_1 by decreasing cyclin D1 and increasing $p27^{Kip1}$ levels

A molecular link between ERK1/2 and STAT3 to proliferation is through cyclin D1 to regulate G_1-to-S cell cycle progression. ERK1/2 activity is required for expression of cyclin D1 in the G_1 phase of the cell cycle. Moreover, STAT3 transcriptionally regulates cyclin-D1 by binding to its promoter region [33, 34]. We assessed the level of cyclin D1 in merlin-deficient HSC after a 24h incubation with ponatinib. We found that ponatinib strongly decreased cyclin D1 protein levels in a dose-dependent manner (Figure 5A). These results suggest that ponatinib reduces the viability of merlin-deficient HSC by inhibiting PDGFRα/β-dependent activation of MEK/ERK and STAT3 pathways, leading to decreased cyclin D1 expression.

To test the possibility that the decrease in the viability of merlin-deficient HSC by ponatinib was a consequence of cell-cycle blockage due to reduced cyclin

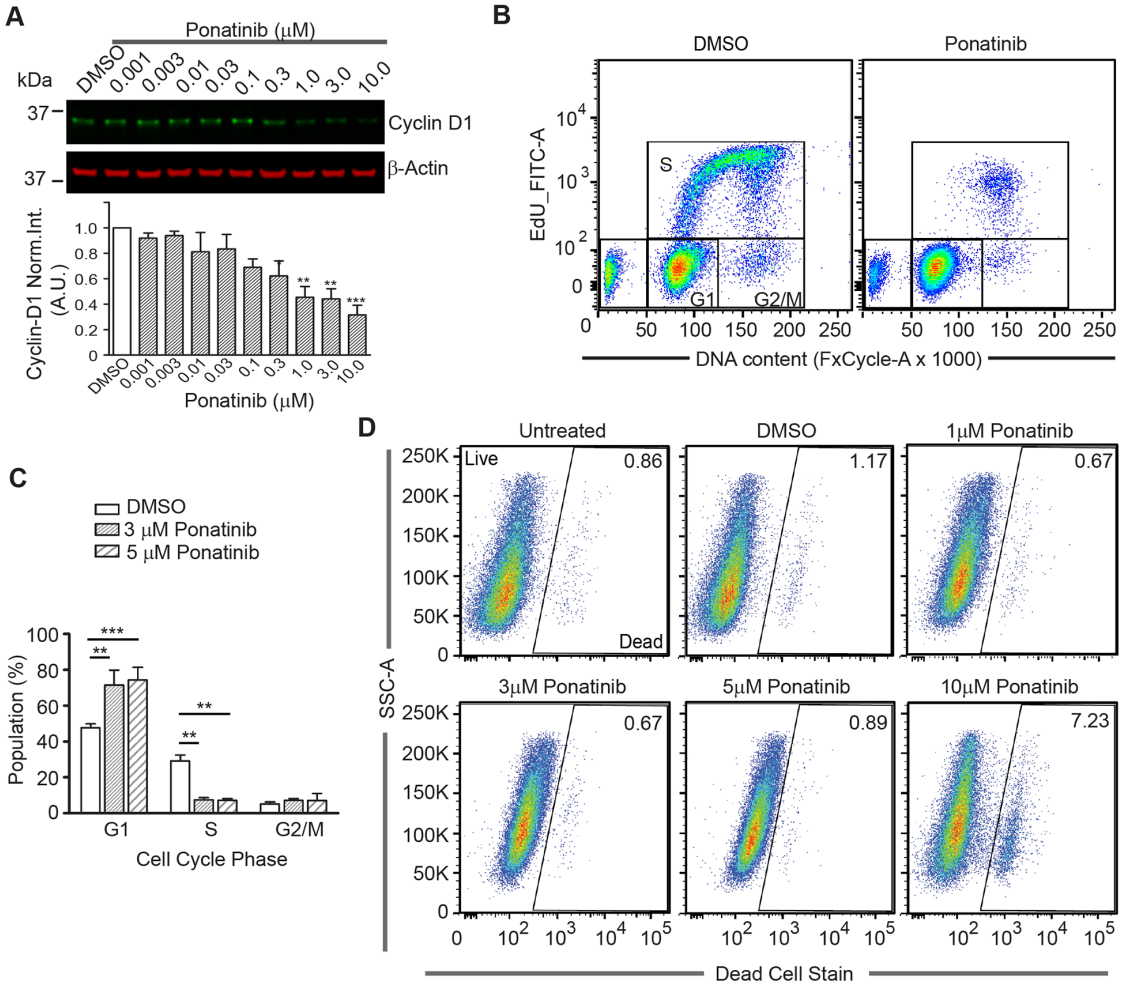

Figure 5: Ponatinib arrests merlin-deficient HSC at the G_1 phase of the cell cycle. **(A)** Representative Western blots for Cyclin D1of lysates prepared from merlin-deficient HSC#45 treated 24h with increasing concentrations of ponatinib. Plotted below as mean ± SEM (n=3). One-way analysis of variance and Dunnett's multiple comparison post-test were used for statistical analysis (** p<0.01 and *** p<0.001). **(B,C)** Merlin-deficient HSC were treated with 3 and 5μM ponatinib for 24h and during the last 3h, 10μM EdU was added. Cells were harvested, labeled with live/dead fixable dye, and analyzed by flow cytometry. **(B)** Representative plots of the distribution of EdU- and FxCycle-labelled cells of 0.1% DMSO vehicle control and ponatinib treated cells. **(C)** Graph of the distribution of the cell cycle phases (gated for the live population) of all the experiments as mean ± SEM, n=4; **p<0.01 and ***p<0.001 were determined by two-way ANOVA and Bonferroni multiple comparisons post-test. **(D)** Representative plots of the distribution of live and dead cell population in these experiments with increasing concentrations of ponatinib as indicated.

D1 expression, we analyzed the distribution of cells among the different phases of the cell cycle. There was a significant increase in the number of cells in the G_1 phase when treated with 3 and 5μM ponatinib compared to vehicle controls (72% ±8% and 74% ±7% vs. 47% ±2% of control). This was accompanied by a concomitant decrease in the number of S-phase cells observed in ponatinib-treated samples as compared with control samples (7.5% ±1% for 3μM and 7% ±1% at 5μM vs. 29% ±3% of control) (Figure 5B–5C). At the lower concentrations (1 through 5μM), ponatinib arrested merlin-deficient HSC at $G_{1,}$ indicating a cytostatic mechanism of action. However,

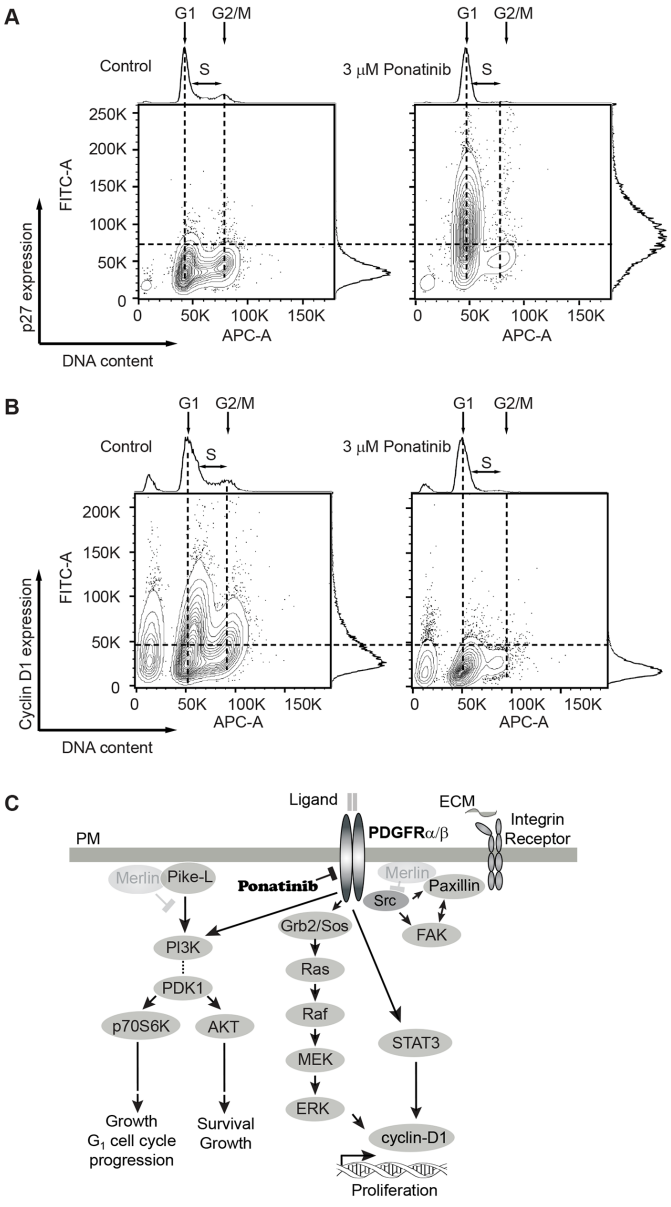

Figure 6: Analysis of G1 regulatory proteins during the cell-cycle in merlin-deficient HSC treated with ponatinib. MD-HSC were treated with 3μM ponatinib or vehicle control for 24h. Cells were harvested, fixed, and permeabilized. DNA was stained with FxCycle, and intracellular G_1 regulatory proteins were immunostained and analyzed by flow cytometry. **(A)** Distribution plots of cells with positive/negative $p27^{Kip1}$ immunostain vs DNA content. Data shown are representative plots of four independent experiments. **(B)** Distribution of cells analyzed by flow cytometry with positive/negative cyclin D1 immunostain vs DNA content. Shown are representatives of four independent experiments. **(C)** Diagram of signaling pathways inhibited by ponatinib in merlin-deficient HSC. Merlin deficiency leads to activation of PDGFR, SRC and PI3K. Activation of PI3K potentiates AKT and p70S6K phosphorylation and leads to cell survival, growth and G_1 cell cycle progression. PDGFR activity triggers ERK and STAT3 activation, leading to cyclin D1 expression and cell proliferation. SRC activation of FAK and paxillin is not modulated by ponatinib. Ponatinib decreases cell viability through downstream inhibition of AKT, ERK, and STAT3.

by analyzing the live/dead populations, at a higher concentration (10μM), ponatinib became cytotoxic (Figure 5D). The increase in the number of dead cells present in the cells treated with 10μM ponatinib coincides with the decrease in phosphorylated proteins studied here.

Lastly, we analyzed the correlation of the cell-cycle phases with levels of several cell cycle regulators. Cyclin-dependent kinase (Cdk) inhibitor p27 ($p27^{Kip1}$) is a key negative regulator of Cdk activity in cells progressing from G_1 toward S phase [35]. We analyzed the expression of $p27^{Kip1}$ in conjunction with DNA content by flow cytometry. We found fewer $p27^{Kip1}$-positive cells in G_1 in control cells compared with a large increase in $p27^{Kip1}$-positive cells in G_1 in ponatinib-treated samples (Figure 6A). Similarly, we found a greater number of cyclin D1-positive cells in control samples in G_1 in contrast to ponatinib-treated samples (Figure 6B). This result correlates with that observed from the Western blot experiment (Figure 5A). Overlay of the $p27^{Kip1}$ and cyclin D1 plots with the cell-cycle plots clearly demonstrate that ponatinib induced G_1 arrest with associated changes in the cyclin D1 and $p27^{Kip1}$ levels in merlin-deficient HSC (Supplementary Figure 3AB). Our results are consistent with ponatinib inhibition of PDGFR and downstream PI3K activity leading to a G_1 cell-cycle arrest of merlin-deficient HSC by blocking ERK- and STAT3-dependent expression of cyclin D1 (Figure 6C).

PDGFRα/β, SRC, STAT 3 and MEK1/2 are highly phosphorylated in human vestibular schwannomas

To assess activation of PDGFRα/β and SRC in human schwannomas, we surveyed a phospho-proteome profile comparing five human vestibular schwannoma specimens with primary normal adult human Schwann cells cultured in the presence of mitogens to stimulate their proliferation. Analysis of phospho-receptor tyrosine kinase and phospho-kinases proteome profiler arrays revealed that schwannomas consistently had higher levels of phosphorylated PDGFRα, PDGFRβ, SRC, MEK and STAT3 compared with control primary HSC (Figure 7 A-D). Schwannomas exhibited averaged 6.6 times higher PDGFRα phosphorylation, 5.4 times higher PDGFRβ phosphorylation, 30 times higher SRC phosphorylation, 5.6 times higher MEK phosphorylation and 7.4 times higher STAT3 phosphorylation compared with control primary HSC (Figure 7 A-D).

DISCUSSION

In this study, we evaluated whether ponatinib, a BCR-ABL/SRC inhibitor approved for use in leukemia, could potentially be repurposed for treatment of NF2 schwannomas. Following merlin depletion, HSC increased the levels of phosphorylated SRC and PDGFRα/β, in agreement with studies in primary human NF2 schwannoma cells [36]. Ponatinib stimulated a robust G_1 cell cycle arrest of merlin-deficient HSC in a dose-dependent manner by inhibiting PDGFRα/β and its downstream effectors AKT, p70S6 kinase, MEK/ERK and STAT3, leading to reduced levels of cyclin D1 and increased levels of $p27^{Kip1}$. Intriguingly, ponatinib did not reduce ABL/SRC/FAK/paxillin net phosphorylation in merlin-deficient HSC. We did not find clear evidence of ABL and SRC inhibition in merlin-deficient HSC treated with ponatinib. However, we found that ponatinib induced a dose-dependent increase in the SRC levels in the HSC. Similar results been reported for SRC inhibition with AZD0530 of Philadelphia chromosome-positive leukaemia cell lines. We speculate that this is due to a compensatory feedback mechanism, suggesting SRC kinase inhibition by ponatinib [37]. Other SRC family members, such as Fyn and Yes, did not change their protein levels in ponatinib-treated cells. In some CML cases of imatinib resistance, upregulation of SRC kinase has been implicated as a BCR-ABL-independent mechanism responsible for imatinib failure [38-40]. Therefore the increase in SRC protein levels observed ponatinib-treated HSC may be an adaptive response. It would be interesting to investigate if other SRC inhibitors, including SU6656, that have anti-proliferative activity in primary human schwannoma cells, also increase SRC levels [20, 41].

Ponatinib lacked selectivity for the merlin-deficient HSC over *NF2* wild-type HSC when cultured in the presence of serum and mitogens. This is comparable to results reported by others with the MEK1 inhibitor AZD6244 in primary human schwannoma cells and normal Schwann cells grown in serum-containing medium [21]. Notably, when cells were incubated in growth arresting medium (SCM base + N2 supplement) in the presence of 0.25 μM ponatinib for one week, merlin-deficient HSC showed a greater sensitivity to the drug than merlin-expressing HSC. To maintain fetus derived cell lines amenable to drug discovery studies, we routinely culture these embryonic Schwann cells in the presence of serum and other mitogenic supplements, which induces Schwann cells to proliferate. In contrast, both myelinating and non-myelinating Schwann cells are post-mitotic in normal nerves [42-44]. Only after nerve injury do adult Schwann cells de-differentiate and proliferate as part of the nerve repair process [21, 45-48]. Thus, ponatinib's lack of *in vitro* selectivity is not a cause for concern for *in vivo* studies and its potential as a therapeutic for NF2-associated schwannomas.

Ponatinib strongly inhibited PDGFR phosphorylation in merlin-deficient HSC. Studies with other RTK inhibitors that primarily target PDGFR and c-KIT (e.g., nilotinib, imatinib and sorafenib) showed that these RTK inhibitors exhibited strong anti-proliferative activity on primary human schwannoma and HEI-193 cells [10, 12, 41]. Merlin was shown to promote the

internalization of activated PDGFRβ, a role consistent with increased expression and activation of mitogenic receptors in NF2 schwannomas [13, 14]. In Schwann cells, PDGFRα and β signaling are central to cell proliferation and survival through the Ras/Raf/MEK/ERK and PI3K/AKT signaling pathways [49-51]. In the four schwannoma samples with chronic merlin loss, the p-AKT Ser473 levels downstream of mTORC2 were reported as consistently reduced across tumor samples relative to normal arachnoid and meningioma tissues, as well as in one immortalized human SC line with acute loss of merlin achieved by an RNAi compared to the immortalized human merlin-expressing SC line [52]. The consistent decrease in mTORC2 signaling activity in schwannoma and merlin-deficient Schwann cells mimics the PDGFR activity results in schwannomas reported by others and our phospho-receptor tyrosine kinase arrays showing a high PDGFR phosphorylation levels in all tumors tested (Figure 7 and 1) [10-12]. Consistent with PDGFR inhibition, we observed a dose-dependent decrease in AKT-Thr308

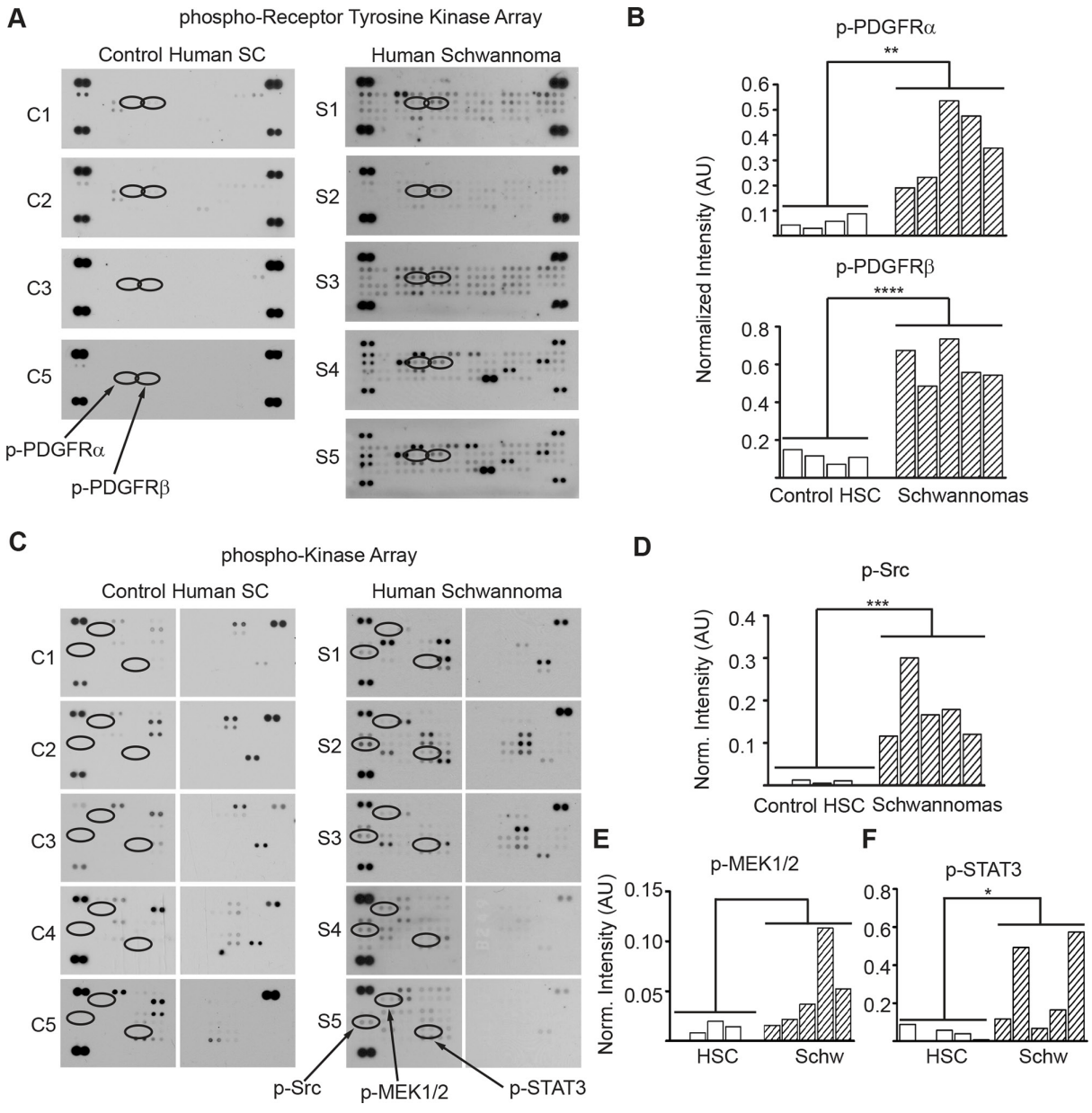

Figure 7: PDGFRα/β, SRC, MEK and STAT3 are overactive in human schwannomas. (A) Phospho-RTK membrane profile of schwannomas and control cultured primary HSC. **(B)** Bar graph of the quantitation ofp-PDGFRα and p-PDGFRβ membrane dot intensity normalized to positive controls. ***p*<0.005; *****p*<0.0001 determined using unpaired *t*-test of control HSC vs. VS populations, two-tailed. **(C)** Phospho-kinase membrane profile of schwannomas and control cultured primary HSC samples. **(D)** Bar graph of the quantitation of phospho-SRC, phospho-MEK1/2 and phospho-STAT3 membrane intensity normalized to positive controls. **p<0.05;* ****p*<0.001 determined using unpaired *t*-test of control HSC vs. VS populations, two-tailed.

phosphorylation, a PI3K-dependent phosphorylation site, and a decrease in MEK/ERK phosphorylation, similar to those reported in sorafenib-treated schwannoma cells [10, 53, 54]. Moreover, we demonstrated a dose-dependent reduction of cyclin D1 levels that correlates with STAT3 inactivation. STAT3 induces cyclin D1 transcription by binding its promoter region; and ERK1/2 has plays a critical role for induction of cyclin D1 (Figure 6C) [33, 34, 55, 56]. Decreased cyclin-D1 expression together with an increase in the $p27^{Kip1}$ level are key to the G_1 to S phase progression block that we observed in ponatinib-treated HSCs.

Unlike traditional dual SRC/ABL inhibitors, ponatinib is a reversible, third-generation inhibitor that binds the unphosphorylated inactive DFG-out conformation of both enzymes [57]. Ponatinib was designed to overcome resistance-inducing BCR-ABL mutations in CML and ALL treated with the first- and second-generation TK inhibitors. It is considered a pan-BCR-ABL inhibitor because it is potently active on ABL-T315I and fourteen other mutants [19]. Ponatinib shows inhibitory activity against ABL/SRC, PDGFR and other kinases, including the FGFR (fibroblast growth factor receptor), Ephrin receptors, FLT3 (FMS-like tyrosine kinase 3), VEGFR1-3 (vascular endothelial growth factor receptor 1-3), Ret (rearranged during transfection) and KIT (mast/stem cell growth factor receptor) [19]. Ponatinib therapy, similar to other TK inhibitors, is associated with severe adverse events, such as arterial thrombosis and liver toxicity, and older patients (>65 years) had higher risk of experiencing adverse effect than younger patients [58, 59]. In a large group of children and adolescents with CML treated with imatinib, assessment of long term growth revealed growth deceleration in both genders [60]. Therefore, adverse effects of long-term treatment in children should be carefully weighed.

Whereas short-term treatment with ponatinib leads to cytostasis, prolonged treatment could lead to cell death or senescence [61, 62]. These sequelae have been reported for B precursor or T cells from ALL patients treated with ponatinib; the treated cells underwent apoptosis after a G_1 cell-cycle arrest by increasing endogenous TNF-related apoptosis-inducing ligand (TRAIL) [63]. Drugs that simply slow schwannoma growth would benefit NF2 patients enormously. If a long-term use of ponatinib is envisioned, we speculate that ponatinib may be used at lower doses in a combinatorial therapeutic approach with other compounds targeting interconnecting pathways, thereby limiting adverse effects. The different mechanisms of kinase inhibition and diverse range and selectivity of small-molecule kinase inhibitors requires that each drug be studied in NF2-relevant cell types, and weighed independently. To this extent, ponatinib treatment effectively reduced viability of merlin-deficient HSC with a robust arrest at the G_1 phase. Ponatinib therapy may be applicable to a larger patient population than NF2, considering that merlin inactivation also occurs in sporadic schwannomas. Future *in vivo* studies addressing ponatinib alone or in combination as an effective therapy for schwannomas in NF2 mouse models are warranted.

MATERIALS AND METHODS

Cell cultures and human vestibular schwannomas

The merlin-deficient HSC line was generated from primary fetal HSC purchased from ScienCell (lot #7228) and authenticated by immunostaining for expression of human nuclear antigen, and SC markers, S100, PLP, O4, and Gap43, and Nestin. Cells were transduced with lentiviral particles expressing human *NF2* gene-specific shRNA (GenBank accession no. NM_000268; TRCN0000237845; TRCN0000039974; TRCN0000039975 and TRCN0000039977, Sigma-Aldrich), shRNA Scrambled, or Turbo-GFP control (Sigma-Aldrich) and then selected with 0.5 mg/ml puromycin. Wild-type and merlin-deficient HSC were cultured in CellBIND dishes (Corning) in complete Schwann cell media (SCM) from ScienCell (basal Schwann cell medium plus 5% fetal bovine serum, Schwann cell growth supplements which contains growth factors, hormones, and proteins necessary for the culture of normal human Schwann cells and 1X-penicillin/streptomycin) unless otherwise specified. Cells were used between passages 9 to 18. Merlin levels were assessed by Western blotting.

Frozen human schwannomas used in phospho-proteome studies were procured with patient informed consent at The Ohio State University College of Medicine according to Institutional Review Board regulations. Human vestibular schwannoma (VS) cells cultured to test ponatinib efficacy were isolated from dissociated fresh human tumors. Fresh VS specimens were procured with patient informed consent at University of Miami Miller School of Medicine according to Institutional Review Board regulations through the Tissue Bank Core Facility.

Normal primary human SCs, a gift from Dr. Patrick Wood (The Miami Project to Cure Paralysis, University of Miami Miller School of Medicine), were used in phospho-proteome studies, and cultured as previously described [64].

Antibody proteome profiler arrays

Human phospho-RTK (ARY001) and phospho-kinase array (ARY003) kits were purchased from R&D systems. Human schwannoma homogenates and control HSC lysates were prepared and analyzed according to manufacturer's instructions. Arrays were visualized with chemiluminescence and were quantified with ImageJ MicroArray_Profile.jar plugin or Carestream software; mean intensity of duplicate spots was calculated.

Antibodies and inhibitors

Rabbit antibodies against merlin (D1D8), c-ABL, phospho-AKT (Thr308; C31E5E), cyclin-D1 (92G2), FYN, p-MEK1/2 (Ser217/221), PDGFRα and β, SRC (36D10), p-SRC family (Tyr416), p-ERK1/2 (D13.14.4E), YES and mouse antibodies recognizing AKT (40D4), β-Actin (8H10D10), MEK1/2 (L38C12), ERK1/2, $p27^{Kip1}$ (SX53G8.5) were purchased from Cell Signaling. Rabbit antibodies against p-paxillin (Tyr118) and p-FAK (Tyr577/Tyr576) were purchased from Invitrogen. Rabbit p70 S6 kinase (Thr229) was purchased form ThermoFisher Scientific. Rabbit anti-p-ABL (Tyr245), and human nuclear antigen antibodies were obtained from Millipore and antibodies for myelin- proteolipid protein and GAP43 were from Abcam. The anti-S100 antibody was purchased from Dako. Mouse anti-paxillin antibody was from BD bioscience. Secondary antibodies, goat anti-rabbit IgG conjugated with DyLight 800 4X-PEG, goat anti-Mouse IgG conjugated with DyLight 680, were purchased from Cell Signaling. Ponatinib, perifosine/KRX-0401, and selumetinib/AZD6244 were purchased from SelleckChem. The STAT3 inhibitor S3I-201/NSC-74859 was purchased from MedChem Express.

Western blot analysis

Cultured HSCs were lysed in modified RIPA buffer as previously described [65] or in 1X-SDS loading buffer plus 2.5 U/ml benzonase. 10 µg of protein or 10 µl 1X-loading buffer lysate were resolved in 4–20% polyacrylamide gels (Pierce), transferred to PVDF membranes (Immobilon-FL; Millipore), blocked with 5% BSA in TBS, and incubated with primary antibodies overnight at 4°C, and then with their corresponding fluorescence-conjugated secondary antibodies at 1:25,000-1:40,000 dilution. Image acquisition was done using LI-COR® Biosciences Odyssey® Infrared Imaging System and quantification using Odyssey Image Studio Version 3.1software and ImageJ 1.46r.

Immunocytochemistry

Cells were grown on German glass coverslips coated with 200 µg/ml poly-L-lysine (Sigma-Aldrich). HSCs were fixed in 4% paraformaldehyde and immunostained, and stained images were acquired with a Zeiss LSM710 confocal microscope as previously described [64]. Images were processed with ZEN2011 software.

Cell viability assay

HSC were seeded at 2,500 cells/well in 20 µl of phenol-red free SCM (SCM phenol-red free base, 5% serum, Schwann cell growth supplements containing growth factors, hormones, and proteins and 1X-penicillin/streptomycin) in 384-well plates and incubated with increasing concentrations of ponatinib in 0.1% DMSO or vehicle alone for 48h. The CellTiter-Fluor cell viability assay (Promega) was used according to manufacturer's specifications [53].

To evaluate cell viability without artificially stimulating proliferation, control and merlin-deficient HSC were cultured and assayed in growth suppressive medium (SCM base, 1X-penicillin/streptomycin –ScienCell, plus N2 supplement-Invitrogen). Cells were seeded in 24 well plates (Corning-CellBIND) at 60,000 cells/well in four replicates, after 4 days incubation at 37°C, 7% CO_2, cells were treated with 0.25µM ponatinib or a vehicle control for one week. Viability was assessed with a crystal violet assay as previously described [64].

To evaluate cell viability of primary VS cells with *NF2* mutations, two fresh VS were obtained from the Tissue Bank Core Facility at the University of Miami Miller School of Medicine. VS tumors were cut into 1 mm pieces and dissociated in 0.5 mg/ml collagenase (~150U/ml) and dispase (2.5 mg/ml) in Dulbecco's Modified Eagle Medium (Sigma) for 1h followed by 0.25% Trypsin for 30 minutes at 37°C. Digested tissue was triturated and centrifuged at 1500 rpm at 4°C for 10 minutes. Supernatant was discarded and cells were resuspended and cultured using Schwann Cell Media (ScienCell) on culture flasks pre-treated with 0.1% poly-L-lysine (Sigma) and 25 mg/ml laminin (ThermoScientific). Cells from Passage 2 were then seeded in a 96 well plate (Costar, Corning) at 5,000 cells/well in six replicates. After 24 hours of incubation at 37°C, 5% CO2, cells were treated with ponatinib at different concentrations or 0.05% DMSO for 48h. Viability was assessed with a crystal violet assay as previously described [64].

DNA sequencing of VS

Genomic DNA was isolated and purified using Trizol (Invitrogen) as per the manufacturer's protocol. A total of 17 pairs of primers were designed for the amplification and sequencing of the coding exons and their flanking splice sites using the Primer 3 program (http://bioinfo.ut.ee/primer3-0.4.0/). The complete coding sequences of *NF2* were amplified by PCR. DNA (~1 µg) was amplified with *NF2*-specific primer pairs in 50µL, containing 10X PCR Buffer (pH 8.5), 0.4 mM dNTP mix (Promega Corporation), 0.4 pmol/µL of each primer, and 0.0625 units of *Taq* DNA polymerase (Eppendorf AG). DNA templates were amplified using the following program: 95°C for 3 min; 35 cycles of 94°C for 50 s, 60°C for 50 s, 72°C for 60 s; and final extension of 72°C for 5 min. Direct sequencing of PCR products were performed on both strands using the ABI Prism BigDye Terminator reaction kit and ABI 3100 DNA sequencer or with Beckman Coulter 2000 XL instrument and appropriate kits.

Cell-cycle and G_1 proteins analysis by flow cytometry

The Click-iT EdU, FxCycle stain and Live/Dead fixable dead cell stain kits were purchased from Molecular Probes (ThermoFisher Scientific). Cells were seeded in 6-well plates and treated overnight with an inhibitor or vehicle. On the next day, 10 μM EdU was added to the cultures for 3 h, and then cells were harvested (total 24-h inhibitor incubation), stained with fixable violet live/dead stain, and permeabilized. EdU and DNA labeling was conducted according to manufacturer's instruction. Cell cycle analysis was done on gated live cells. For the cyclin D1/$p27^{Kip1}$ expression study [66], cultures were treated with an inhibitor or vehicle for 24 h and then harvested, fixed with 4% paraformaldehyde for 10 min at 37°C, chilled for 1 min, and permeabilized for 30 min in 90% methanol. Fixed cells were transferred to a Falcon 5 ml tube through a cell strainer cap, rinsed twice with 0.5% BSA in PBS, and immunostained by incubating for 1h at room temperature with a cyclin D1 (1:400) or $p27^{Kip1}$ (1:3,000) antibody, followed by a 30-min incubation with a goat anti-rabbit or anti-mouse-Alexa488 secondary antibody. After one wash, cells were resuspended in 1 ml of 0.5% BSA and stained for 30 min with 200nM FxCycle Far Red DNA stain supplemented with 0.1mg/ml of ribonucleaseA (Invitrogen). A BD FACS Canto-II flow cytometer (BD Biosciences) with the BD FACSDiva™ 6.1.3 software was used for data acquisition and FlowJo software was used for data analysis.

Statistical analysis

Statistical analysis was performed using GraphPad Prism v5.0 for Windows. Ponatinib dose-response experiments were analyzed by non-linear regression (four parameters). Other experiments were analyzed by applying two-way ANOVA and Bonferroni multiple comparisons post-test, one-way ANOVA, and Dunnett's multiple comparison post-test or unpaired *t*-test, two-tailed as noted.

Author contributions

A.M.P. designed experiments, performed research, analyzed and interpreted data, and wrote the manuscript; J.G., M.B., S.K.P., O.R.B., B.Z. and R.M. performed research and analyzed data; C.T.D., D.Y., F.F.T., X.Z.L., L.S.C., D.B.W., and A.J.C. designed experiments, analyzed data, contributed to intellectual development of the manuscript, and revised the manuscript; C.F.V. supervised the project, analyzed data, and wrote the manuscript.

ACKNOWLEDGMENTS

We thank Dr. Michael Ivan and Dr. Jacques Morcos for their generosity and time harvesting tumors. We thank Drs. Annette Khaled and Deborah Altomare for helpful discussions, and Jeremiah Oyer for assistance with flow cytometry.

CONFLICTS OF INTEREST

The authors reported no potential conflicts of interest.

GRANT SUPPORT

This work was supported by a Department of Defense (NF140044 to CFV and NF150080 to LSC) and a Children's Tumor Foundation Drug Discovery Award 2014 to CFV. JG received support from UCF's Office of Undergraduate Research.

REFERENCES

1. Blakeley JO, Plotkin SR. Therapeutic advances for the tumors associated with neurofibromatosis type 1, type 2, and schwannomatosis. Neuro-oncology. 2016; 18:624-38.
2. Rouleau GA, Merel P, Lutchman M, Sanson M, Zucman J, Marineau C, Hoang-Xuan K, Demczuk S, Desmaze C, Plougastel B, et al. Alteration in a new gene encoding a putative membrane-organizing protein causes neuro-fibromatosis type 2. Nature. 1993; 363:515-521.
3. Trofatter JA, MacCollin MM, Rutter JL, Murrell JR, Duyao MP, Parry DM, Eldridge R, Kley N, Menon AG, Pulaski K, et al. A novel moesin-, ezrin-, radixin-like gene is a candidate for the neurofibromatosis 2 tumor suppressor. Cell. 1993; 72:791-800.
4. Petrilli AM, Fernandez-Valle C. Role of Merlin/NF2 inactivation in tumor biology. Oncogene. 2015; 35:537-48.
5. Farschtschi S, Kollmann P, Dalchow C, Stein A and Mautner VF. Reduced dosage of bevacizumab in treatment of vestibular schwannomas in patients with neurofibromatosis type 2. Eur Arch Otorhinolaryngol. 2015; 272:3857-3860.
6. Karajannis MA and Ferner RE. Neurofibromatosis-related tumors: emerging biology and therapies. Current opinion in pediatrics. 2015; 27:26-33.
7. Ammoun S and Hanemann CO. Emerging therapeutic targets in schwannomas and other merlin-deficient tumors. Nature reviews Neurology. 2011; 7:392-399.
8. Andrae J, Gallini R and Betsholtz C. Role of platelet-derived growth factors in physiology and medicine. Genes Dev. 2008; 22:1276-1312.
9. Roskoski R, Jr. Src protein-tyrosine kinase structure, mechanism, and small molecule inhibitors. Pharmacol Res. 2015; 94:9-25.

10. Ammoun S, Flaiz C, Ristic N, Schuldt J and Hanemann CO. Dissecting and targeting the growth factor-dependent and growth factor-independent extracellular signal-regulated kinase pathway in human schwannoma. Cancer Res. 2008; 68:5236-5245.
11. Lallemand D, Manent J, Couvelard A, Watilliaux A, Siena M, Chareyre F, Lampin A, Niwa-Kawakita M, Kalamarides M and Giovannini M. Merlin regulates transmembrane receptor accumulation and signaling at the plasma membrane in primary mouse Schwann cells and in human schwannomas. Oncogene. 2009; 28:854-865.
12. Mukherjee J, Kamnasaran D, Balasubramaniam A, Radovanovic I, Zadeh G, Kiehl TR and Guha A. Human schwannomas express activated platelet-derived growth factor receptors and c-kit and are growth inhibited by Gleevec (Imatinib Mesylate). Cancer Res. 2009; 69:5099-5107.
13. Ammoun S, Cunliffe CH, Allen JC, Chiriboga L, Giancotti FG, Zagzag D, Hanemann CO and Karajannis MA. ErbB/HER receptor activation and preclinical efficacy of lapatinib in vestibular schwannoma. Neuro-oncology. 2010; 12:834-843.
14. Fraenzer JT, Pan H, Minimo L, Jr., Smith GM, Knauer D and Hung G. Overexpression of the NF2 gene inhibits schwannoma cell proliferation through promoting PDGFR degradation. Int J Oncol. 2003; 23:1493-1500.
15. Houshmandi SS, Emnett RJ, Giovannini M and Gutmann DH. The neurofibromatosis 2 protein, merlin, regulates glial cell growth in an ErbB2- and Src-dependent manner. Molecular and cellular biology. 2009; 29:1472-1486.
16. Zhou L and Hanemann CO. Merlin, a multi-suppressor from cell membrane to the nucleus. FEBS Lett. 2012; 586:1403-1408.
17. Zhou T, Commodore L, Huang WS, Wang Y, Thomas M, Keats J, Xu Q, Rivera VM, Shakespeare WC, Clackson T, Dalgarno DC and Zhu X. Structural mechanism of the Pan-BCR-ABL inhibitor ponatinib (AP24534): lessons for overcoming kinase inhibitor resistance. Chem Biol Drug Des. 2011; 77:1-11.
18. Blanc J, Geney R and Menet C. Type II kinase inhibitors: an opportunity in cancer for rational design. Anticancer Agents Med Chem. 2013; 13:731-747.
19. O'Hare T, Shakespeare WC, Zhu X, Eide CA, Rivera VM, Wang F, Adrian LT, Zhou T, Huang WS, Xu Q, Metcalf CA 3rd, Tyner JW, Loriaux MM, et al. AP24534, a pan-BCR-ABL inhibitor for chronic myeloid leukemia, potently inhibits the T315I mutant and overcomes mutation-based resistance. Cancer Cell. 2009; 16:401-412.
20. Zhou L, Ercolano E, Ammoun S, Schmid MC, Barczyk MA and Hanemann CO. Merlin-deficient human tumors show loss of contact inhibition and activation of Wnt/beta-catenin signaling linked to the PDGFR/Src and Rac/PAK pathways. Neoplasia. 2011; 13:1101-1112.
21. Ammoun S, Ristic N, Matthies C, Hilton DA and Hanemann CO. Targeting ERK1/2 activation and proliferation in human primary schwannoma cells with MEK1/2 inhibitor AZD6244. Neurobiology of disease. 2010; 37:141-146.
22. Hossain S, Fragoso G, Mushynski WE and Almazan G. Regulation of peripheral myelination by Src-like kinases. Exp Neurol. 2010; 226:47-57.
23. Kumar A, Jaggi AS and Singh N. Pharmacology of Src family kinases and therapeutic implications of their modulators. Fundam Clin Pharmacol. 2015; 29:115-130.
24. McLean GW, Carragher NO, Avizienyte E, Evans J, Brunton VG and Frame MC. The role of focal-adhesion kinase in cancer - a new therapeutic opportunity. Nat Rev Cancer. 2005; 5:505-515.
25. Calalb MB, Polte TR and Hanks SK. Tyrosine phosphorylation of focal adhesion kinase at sites in the catalytic domain regulates kinase activity: a role for Src family kinases. Molecular and cellular biology. 1995; 15:954-963.
26. Turner CE. Paxillin interactions. J Cell Sci. 2000; 113 Pt 23:4139-4140.
27. Heldin CH and Lennartsson J. Structural and functional properties of platelet-derived growth factor and stem cell factor receptors. Cold Spring Harb Perspect Biol. 2013; 5:a009100.
28. Alessi DR, Andjelkovic M, Caudwell B, Cron P, Morrice N, Cohen P and Hemmings BA. Mechanism of activation of protein kinase B by insulin and IGF-1. EMBO J. 1996; 15:6541-6551.
29. Alessi DR, Kozlowski MT, Weng QP, Morrice N and Avruch J. 3-Phosphoinositide-dependent protein kinase 1 (PDK1) phosphorylates and activates the p70 S6 kinase *in vivo* and *in vitro*. Curr Biol. 1998; 8:69-81.
30. Bowman T, Broome MA, Sinibaldi D, Wharton W, Pledger WJ, Sedivy JM, Irby R, Yeatman T, Courtneidge SA and Jove R. Stat3-mediated Myc expression is required for Src transformation and PDGF-induced mitogenesis. Proc Natl Acad Sci U S A. 2001; 98:7319-7324.
31. Kortylewski M, Jove R and Yu H. Targeting STAT3 affects melanoma on multiple fronts. Cancer Metastasis Rev. 2005; 24:315-327.
32. Wang YZ, Wharton W, Garcia R, Kraker A, Jove R and Pledger WJ. Activation of Stat3 preassembled with platelet-derived growth factor beta receptors requires Src kinase activity. Oncogene. 2000; 19:2075-2085.
33. Kim DJ, Chan KS, Sano S and Digiovanni J. Signal transducer and activator of transcription 3 (Stat3) in epithelial carcinogenesis. Mol Carcinog. 2007; 46:725-731.
34. Meloche S and Pouyssegur J. The ERK1/2 mitogen-activated protein kinase pathway as a master regulator of the G1- to S-phase transition. Oncogene. 2007; 26:3227-3239.
35. Jakel H, Peschel I, Kunze C, Weinl C and Hengst L. Regulation of p27 (Kip1) by mitogen-induced tyrosine phosphorylation. Cell Cycle. 2012; 11:1910-1917.

36. Ammoun S, Schmid MC, Zhou L, Ristic N, Ercolano E, Hilton DA, Perks CM and Hanemann CO. Insulin-like growth factor-binding protein-1 (IGFBP-1) regulates human schwannoma proliferation, adhesion and survival. Oncogene. 2012; 31:1710-1722.

37. Gwanmesia PM, Romanski A, Schwarz K, Bacic B, Ruthardt M and Ottmann OG. The effect of the dual Src/Abl kinase inhibitor AZD0530 on Philadelphia positive leukaemia cell lines. BMC Cancer. 2009; 9:53.

38. Donato NJ, Wu JY, Stapley J, Lin H, Arlinghaus R, Aggarwal BB, Shishodia S, Albitar M, Hayes K, Kantarjian H and Talpaz M. Imatinib mesylate resistance through BCR-ABL independence in chronic myelogenous leukemia. Cancer Res. 2004; 64:672-677.

39. Huang WS, Zhu X, Wang Y, Azam M, Wen D, Sundaramoorthi R, Thomas RM, Liu S, Banda G, Lentini SP, Das S, Xu Q, Keats J, et al. 9-(Arenethenyl) purines as dual Src/Abl kinase inhibitors targeting the inactive conformation: design, synthesis, and biological evaluation. J Med Chem. 2009; 52:4743-4756.

40. Jabbour E, Kantarjian H and Cortes J. Use of second- and third-generation tyrosine kinase inhibitors in the treatment of chronic myeloid leukemia: an evolving treatment paradigm. Clin Lymphoma Myeloma Leuk. 2015; 15:323-334.

41. Ammoun S, Schmid MC, Triner J, Manley P and Hanemann CO. Nilotinib alone or in combination with selumetinib is a drug candidate for neurofibromatosis type 2. Neuro-oncology. 2011; 13:759-766.

42. Giovannini M, Robanus-Maandag E, van der Valk M, Niwa-Kawakita M, Abramowski V, Goutebroze L, Woodruff JM, Berns A and Thomas G. Conditional biallelic Nf2 mutation in the mouse promotes manifestations of human neurofibromatosis type 2. Genes Dev. 2000; 14:1617-1630.

43. Jessen KR, Mirsky R and Morgan L. Role of cyclic AMP and proliferation controls in Schwann cell differentiation. Ann N Y Acad Sci. 1991; 633:78-89.

44. Zorick TS and Lemke G. Schwann cell differentiation. Curr Opin Cell Biol. 1996; 8:870-876.

45. Atanasoski S, Boentert M, De Ventura L, Pohl H, Baranek C, Beier K, Young P, Barbacid M and Suter U. Postnatal Schwann cell proliferation but not myelination is strictly and uniquely dependent on cyclin-dependent kinase 4 (cdk4). Mol Cell Neurosci. 2008; 37:519-527.

46. Mirsky R, Woodhoo A, Parkinson DB, Arthur-Farraj P, Bhaskaran A and Jessen KR. Novel signals controlling embryonic Schwann cell development, myelination and dedifferentiation. J Peripher Nerv Syst. 2008; 13:122-135.

47. Atanasoski S, Shumas S, Dickson C, Scherer SS and Suter U. Differential cyclin D1 requirements of proliferating Schwann cells during development and after injury. Mol Cell Neurosci. 2001; 18:581-592.

48. Kim HA, Pomeroy SL, Whoriskey W, Pawlitzky I, Benowitz LI, Sicinski P, Stiles CD and Roberts TM. A developmentally regulated switch directs regenerative growth of Schwann cells through cyclin D1. Neuron. 2000; 26:405-416.

49. Heldin CH and Westermark B. Mechanism of action and *in vivo* role of platelet-derived growth factor. Physiol Rev. 1999; 79:1283-1316.

50. Meier C, Parmantier E, Brennan A, Mirsky R and Jessen KR. Developing Schwann cells acquire the ability to survive without axons by establishing an autocrine circuit involving insulin-like growth factor, neurotrophin-3, and platelet-derived growth factor-BB. J Neurosci. 1999; 19:3847-3859.

51. Peulve P, Laquerriere A, Paresy M, Hemet J and Tadie M. Establishment of adult rat Schwann cell cultures: effect of b-FGF, alpha-MSH, NGF, PDGF, and TGF-beta on cell cycle. Exp Cell Res. 1994; 214:543-550.

52. James MF, Stivison E, Beauchamp R, Han S, Li H, Wallace MR, Gusella JF, Stemmer-Rachamimov AO and Ramesh V. Regulation of mTOR complex 2 signaling in neurofibromatosis 2-deficient target cell types. Mol Cancer Res. 2012; 10:649-659.

53. Petrilli AM, Fuse MA, Donnan MS, Bott M, Sparrow NA, Tondera D, Huffziger J, Frenzel C, Malany CS, Echeverri CJ, Smith L and Fernandez-Valle C. A chemical biology approach identified PI3K as a potential therapeutic target for neurofibromatosis type 2. American journal of translational research. 2014; 6:471-493.

54. Rong R, Tang X, Gutmann DH and Ye K. Neurofibromatosis 2 (NF2) tumor suppressor merlin inhibits phosphatidylinositol 3-kinase through binding to PIKE-L. Proc Natl Acad Sci U S A. 2004; 101:18200-18205.

55. Masuda M, Suzui M, Yasumatu R, Nakashima T, Kuratomi Y, Azuma K, Tomita K, Komiyama S and Weinstein IB. Constitutive activation of signal transducers and activators of transcription 3 correlates with cyclin D1 overexpression and may provide a novel prognostic marker in head and neck squamous cell carcinoma. Cancer Res. 2002; 62:3351-3355.

56. Sinibaldi D, Wharton W, Turkson J, Bowman T, Pledger WJ and Jove R. Induction of p21WAF1/CIP1 and cyclin D1 expression by the Src oncoprotein in mouse fibroblasts: role of activated STAT3 signaling. Oncogene. 2000; 19:5419-5427.

57. Hari SB, Perera BG, Ranjitkar P, Seeliger MA and Maly DJ. Conformation-selective inhibitors reveal differences in the activation and phosphate-binding loops of the tyrosine kinases Abl and Src. ACS Chem Biol. 2013; 8:2734-2743.

58. Hoy SM. Ponatinib: a review of its use in adults with chronic myeloid leukaemia or Philadelphia chromosome-positive acute lymphoblastic leukaemia. Drugs. 2014; 74:793-806.

59. Moslehi JJ and Deininger M. Tyrosine Kinase Inhibitor-Associated Cardiovascular Toxicity in Chronic Myeloid Leukemia. J Clin Oncol. 2015; 33:4210-4218.

60. Millot F, Guilhot J, Baruchel A, Petit A, Leblanc T, Bertrand Y, Mazingue F, Lutz P, Verite C, Berthou C, Galambrun

C, Nicolas S, Yacouben K, et al. Growth deceleration in children treated with imatinib for chronic myeloid leukaemia. Eur J Cancer. 2014; 50:3206-3211.

61. Mombach JC, Bugs CA and Chaouiya C. Modelling the onset of senescence at the G1/S cell cycle checkpoint. BMC Genomics. 2014; 15:S7.

62. Pucci B, Kasten M and Giordano A. Cell cycle and apoptosis. Neoplasia. 2000; 2:291-299.

63. Ehrhardt H, Wachter F, Grunert M and Jeremias I. Cell cycle-arrested tumor cells exhibit increased sensitivity towards TRAIL-induced apoptosis. Cell Death Dis. 2013; 4:e661.

64. Petrilli A, Copik A, Posadas M, Chang LS, Welling DB, Giovannini M and Fernandez-Valle C. LIM domain kinases as potential therapeutic targets for neurofibromatosis type 2. Oncogene. 2014; 33:3571-3582.

65. Petrilli A, Bott M and Fernandez-Valle C. Inhibition of SIRT2 in merlin/NF2-mutant Schwann cells triggers necrosis. Oncotarget. 2013; 4:2354-2365. doi: 10.18632/oncotarget.1422.

66. Darzynkiewicz Z, Gong J, Juan G, Ardelt B and Traganos F. Cytometry of cyclin proteins. Cytometry. 1996; 25:1-13.

Abstract presented at the 2016 NF Conference, Austin, TX. (Jun. 2016)

Similarities and Differences in Tumor Characteristics and Treatment Response in NF2-Associated Vestibular Schwannomas and Meningiomas

Sarah S. Burns, BA
Nationwide Children's Hospital and The Ohio State University

Neurofibromatosis type 2 (NF2) is characterized by the development of multiple nervous system tumors, including vestibular schwannomas (VS) and meningiomas. These tumors cause considerable morbidities, including profound deafness, tinnitus, facial nerve paralysis, ataxia, and brainstem compression; however, an effective medical therapy is presently not available. Previously, we showed that the histone deacetylase inhibitor (HDACi) AR-42 causes tumor regression and inhibits tumor growth in animal models of *NF2*-deficient meningioma and schwannoma, respectively. Similarly, AR-42 reduced tumor size in meningiomas while slowing the growth of VS in an NF2 patient. To investigate this difference in treatment response, we screened for genetic mutations in 405 cancer-related genes in VS and meningiomas from two NF2 patients treated with AR-42. In addition to mutations in *NF2*, VS from both patients harbored mutations in *NUP98*, which is important for nuclear transport, mitotic checkpoint, and immunity. Also, we detected a duplication of exon 2-3 of the *MYC* gene in one of these patients. Analysis of blood samples from these patients and their parents confirmed that these mutations were present in the germline. Intriguingly, in a patient with multiple tumors, we observed the same genetic changes in both VS and meningiomas, implicating additional factors in treatment response. Interestingly, we detected a significant number of CD163+ macrophages in a majority of meningiomas, whereas little or no macrophages were present in the 20 VS examined. The MYC protein has been shown to regulate tumor microenvironment, which can be affected by HDACi's. Importantly, strong nuclear MYC expression was detected in the majority of VS specimens but not in meningiomas. Experiments are in progress to evaluate MYC inhibitors for their ability to inhibit tumor growth and to enhance sensitivity to AR-42. Our results suggest that targeting tumor microenvironment may enhance therapeutic response in NF2-associated tumors.

Full List Authors: Sarah S. Burns, BA[1,2], Elena M. Akhmametyeva, MD, PhD[1,2], Jaishri Blakeley, MD[4], D. Bradley Welling, MD, PhD[5], and Long-Sheng Chang, PhD[1,2,3]

[1]Center for Childhood Cancer and Blood Diseases, Nationwide Children's Hospital and Departments of [2]Pediatrics and [3]Otolaryngology, The Ohio State University, [4]Departments of Neurology, Neurosurgery, and Oncology, Johns Hopkins University, and [5]Department of Otology and Laryngology, Harvard Medical School and Massachusetts General Hospital

Funding: The Galloway Family, Advocure NF2, Meningioma Mommas, CTF, and the Department of Defense

Abstract presented at the 2016 NF Conference, Austin, TX. (Jun. 2016)

ErbB3 and IGF-1R blockade as a potential treatment for vestibular schwannomas and meningiomas

Janet Oblinger, Ph.D.
Nationwide Children's Hospital & The Ohio State University

Vestibular schwannomas (VS) and meningiomas are intracranial tumors that are frequently caused by inactivation of the *NF2*/merlin tumor suppressor gene. These neoplasms incur significant patient morbidities, such as deafness, vertigo, facial paralysis, hydrocephalus, cranial nerve palsy, seizures, and brainstem compression. Currently, treatments for these tumors include surgical excision or radiation; however, an FDA-approved targeted therapy is not available. One of merlin's functions is to suppress aberrant signaling from receptor tyrosine kinases (RTKs) on the cell surface. Indeed, VS and meningiomas often exhibit abnormal activation of RTKs, including members of the epidermal growth factor receptor (EGFR) family and insulin-like growth factor 1 receptor (IGF-1R). However, the EGFR inhibitors erlotinib and lapatinib exhibit only minimal efficacy in VS or meningioma patients, suggesting that additional RTKs provide survival signals for these tumors. We show that treatment of NF2 patient schwannoma and Ben-Men-1 benign meningioma cells with MM-121, an antibody that targets the EGFR member ErbB3, abrogates ligand-induced receptor activation and AKT phosphorylation. Similarly, treatment with MM-141, a bispecific antibody which blocks ErbB3 and IGF-1R signaling, also reduces activation of these receptors and downstream AKT. Importantly, prolonged treatment with MM-121 or MM-141 strongly suppresses ligand-mediated cell proliferation of NF2 schwannoma cells by 65% and 81%, respectively. We also found that Ben-Men-1 cells possess autocrine ErbB3 activation, which drives robust AKT signaling. Addition of MM-121 or MM-141 to Ben-Men-1 cells reduces ligand-induced cell growth and S-phase entry. These promising results warrant further *in vivo* evaluation of MM-121 and MM-141. Our study implicates ErbB3 and IGF-1R as important in VS and meningioma cell growth and indicates that blockade of these RTKs should be considered in the treatment of these tumors.

Full List Authors: Janet Oblinger[1,2], Sarah Burns[1,2], Michael Curley[4], Long-Sheng Chang[1,2,3]

[1]Center for Childhood Cancer, The Research Institute at Nationwide Children's Hospital, Depts of [2]Pediatrics & [3]Otolaryngology, The Ohio State University, [4]Merrimack Pharmaceuticals, Inc.

Funding: Galloway Family Fund, Advocure NF2, CTF, Department of Defense

Abstract presented at the 2017 NF Conference, Washington, DC. (Jun. 2017)

A strategy to identify an effective therapy for NF2-associated vestibular schwannomas

Janet Oblinger, Ph.D.
Nationwide Children's Hospital & The Ohio State University

Current treatment options for neurofibromatosis type 2 (NF2)-associated vestibular schwannomas (VS) and meningiomas are limited to surgery and radiation; however, serious complications can occur with these treatments, and radiation can induce secondary malignancies. Also, incomplete tumor resection is not uncommon and is a main cause of tumor recurrence. Development of an effective medical therapy for NF2-associated tumors is urgently needed. Previously we reported that while the histone deacetylase inhibitor AR-42 caused tumor regression in *NF2*-deficient meningiomas, it merely inhibited tumor growth in schwannomas. Similar findings were observed in a clinical trial of AR-42 in NF2 patients. Meningiomas treated with AR-42 exhibited tumor regression; in contrast, AR-42 only slowed VS growth. In one patient with multiple tumors, his meningiomas remained small while the growth of his VS rebounded after cessation of AR-42 treatment. These results suggest that a more effective treatment of VS may require a drug combination. To investigate possible underlying causes for the differential response of meningiomas and VS to AR-42, we performed mutational analysis of tumors from two NF2 patients. In addition to *NF2* mutations, VS from both patients harbored mutations in the *NUP98* gene. Also, a duplication of exon 2-3 in the *MYC* gene was detected in one of the patients. Intriguingly, we detected the same genetic changes in the left and right VS and meningioma from the same patient. Immunostaining revealed strong nuclear MYC staining in 20 VS analyzed, but meningiomas showed little nuclear MYC expression. Depletion of MYC by shRNAs suppressed VS but not meningioma cell growth, suggesting that drugs targeting MYC expression may be effective in VS. Consistently, we showed that the bromodomain inhibitor JQ1, which transcriptionally downregulates MYC, inhibited VS cell proliferation. Combining JQ1 with AR-42 resulted in enhanced growth suppression. We are presently investigating additional drug combinations with the ultimate goal of identifying an effective therapy for VS. Further, we have established telomerase-immortalized cell lines from NF2 patient tumors for further investigation.

Full List Authors: Sarah Burns[1,2], Janet Oblinger[1,2], Elena Akhmametyeva,[1,2] D. Bradley Welling,[3,4], Long-Sheng Chang[1,2,3]

[1]Center for Childhood Cancer and Blood Diseases, Nationwide Children's Hospital, Departments of [2]Pediatrics and [3]Otolaryngology, The Ohio State University, and [4]Department of Otolaryngology, Harvard Medical School/Massachusetts General Hospital

Support: The Galloway Family, the Franklin/Goodkind Family, Advocure NF2, CTF, Department of Defense

Abstract presented at the 2017 NF Conference, Washington, DC. (Jun. 2017)

Natural Silvestrol-Related Rocaglates as Potential Treatments for Vestibular Schwannomas and Meningiomas

Janet Oblinger, Ph.D.
Nationwide Children's Hospital & The Ohio State University

Vestibular schwannomas (VS) and meningiomas are intracranial tumors that are often caused by inactivation of the *NF2*/merlin tumor suppressor gene. These tumors cause serious morbidities, including deafness, vertigo, facial paralysis, hydrocephalus, cranial nerve palsies, seizures, and brainstem compression. Currently, surgical excision and radiation are the treatment options for these tumors, since an FDA-approved targeted therapy is not yet available. We and others have previously shown that VS and meningiomas often exhibit high levels of activated AKT, which can promote protein biosynthesis. As uncontrolled growth of tumor cells often requires a high degree of protein translation, we found that both of these tumors frequently over-express eIF4A, eIF4E, and eIF4G, components of the eukaryotic initiation factor 4F (eIF4F) complex that critically regulates protein translation initiation. Intriguingly, the eIF4A inhibitor silvestrol, which is a member of the rocaglate family isolated from *Aglaia* plants in tropical rainforests, was consistently found to be a potent inhibitor of VS and meningiomas. However, due to its complex structure and large molecular weight, silvestrol has suboptimal pharmacokinetic and pharmacodynamic properties. To this end, we have investigated the growth-inhibitory activity of 10 silvestrol-related compounds isolated from *Aglaia perviridis*. These compounds have the same scaffold as silvestrol, but lack the bulky, sugar-like dioxanyl ring that is thought to hinder silvestrol's bioavailability. We found that three of these silvestrol related rocaglates, didesmethylrocaglamide, methyl 4′-demethoxy-3′,4′-methylenedioxyrocaglate, and rocaglaol, strongly inhibited the growth of schwannoma and meningioma cells with IC_{50} values similar to or better than that of silvestrol (less than 100 nM). Importantly, the IC_{50} values for these rocaglates in normal meningeal cells were greater than 300 nM, suggesting an improved therapeutic window. Like silvestrol, didesmethylrocaglamide and rocaglaol decreased the levels of phospho-AKT, PCNA, cyclin D1, and Aurora A. Studies are in progress to verify the *in vivo* efficacy of these compounds in our tumor models.

Full List Authors: Janet Oblinger[1,2], Sarah Burns[1,2], A. Douglas Kinghorn[4], Long-Sheng Chang[1,2,3]

[1]Center for Childhood Cancer and Blood Diseases, The Research Institute at Nationwide Children's Hospital, Departments of [2]Pediatrics & [3]Otolaryngology, The Ohio State University, [4]Division of Medicinal Chemistry and Pharmacognosy, College of Pharmacy

Funding: Advocure NF2, the Galloway Family, CTF, and the Department of Defense

Abstract presented at the 2017 NF Conference, Washington, DC. (Jun. 2017)

Merlin plays an important role in centrosome disjunction

Long-Sheng Chang, PhD
Nationwide Children's Hospital and The Ohio State University

Neurofibromatosis type 2 (NF2) is a genetic disorder characterized by the development of multiple nervous system tumors, such as vestibular schwannomas. NF2 is caused by mutations in the *NF2* gene, which encodes the merlin protein that regulates multiple signaling pathways in several cellular compartments. In addition, somatic *NF2* mutations have been detected in multiple cancer types, including breast cancer. Presently, the mechanism by which *NF2* inactivation leads to tumorigenesis is not completely understood. We have shown that *NF2* is strongly expressed in the developing brain and in regions containing migrating cells, including the neural tube closure. Using *Nestin-CreER*, we demonstrated that *Nf2* inactivation during early gestation impaired neuroprogenitor cell proliferation and caused neural tube defects. In contrast, mice with *Nf2* inactivation during mid-to-late gestation developed schwannomas at a high frequency. Similarly, we showed that *Nf2* inactivation in luminal epithelial cells during mid-to-late pregnancy using *Wap1-Cre* and during early pregnancy using *Blg-Cre* markedly decreased cell proliferation, leading to impaired lobuloalveolar morphogenesis. Interestingly, 100% of these mice with *Nf2* knockout in mammary epithelial cells developed mammary tumors following multiple gestation cycles. The decreased cell proliferation during development and tumor formation at later stages due to *Nf2* loss in neural and mammary epithelial cells implies that merlin either inhibits or supports cell proliferation depending on the biological context. To further examine the role of merlin during tumorigenesis, we found that mitotic neuroprogenitor and mammary epithelial cells lacking *Nf2* displayed abnormal spindle formation and chromosome segregation due to defects in centrosome duplication and separation. We have generated merlin-deficient MCF10A mammary epithelial cells using shRNA or the CRISPR/Cas 9 technology. Both *NF2*-depleted and *NF2*-null MCF10A cells also exhibited abnormal centrosome separation, resulting in abnormal centrosome clustering or multiple centrosome formation. Double immunostaining detected merlin in the centrosomes. As β-catenin is a Nek2 substrate involved in centrosome separation, we found that depletion of merlin affected β-catenin phosphorylation at the centrosome. Together, these results suggest that merlin plays an important role during the centrosome separation process. Experiments are in progress to examine possible therapeutic implications of our findings.

Full List Authors: Long-Sheng Chang,[1,2,3] Jie Huang,[1,2] Elena Akhmametyeva,[1,2] Sarah Burns[1,2]
[1]The Research Institute at Nationwide Children's Hospital and [2]Department of Pediatrics, The Ohio State University

Funding: the Department of Defense. We sincerely thank Dr. Marco Giovannini for *Nf2*$^{flox/flox}$ mice.